The thermo-mechanical behaviour of the Callovo-Oxfordian claystone

Hamza Menaceur, Pierre Delage, Anh Minh A.M. Tang, Nathalie Conil

On the thermo-mechanical behaviour of the Callovo-Oxfordian claystone

Hamza MENACEUR[1], Pierre DELAGE[1], Anh-Minh TANG[1], Nathalie CONIL[2]

[1] *Ecole des Ponts ParisTech, Navier/CERMES, France*

[2] *Andra, Bure, France*

Corresponding author:

Pierre Delage

Laboratoire Navier/CERMES

Ecole des Ponts ParisTech

6-8 av. Blaise Pascal

77455 MARNE-LA-VALLEE

France

Tel : +33.1.64.15.35.42

Fax : +33.1.64.15.35.62

Email : pierre.delage@enpc.fr

Abstract:

The Callovo-Oxfordian (COx) claystone is considered as a potential host rock in the French concept of high level radioactive waste disposal at great depth. To better understand and to complement existing published data on the thermo-hydro-mechanical behaviour of the COx claystone, an experimental program was carried out by using a hollow cylinder triaxial device specially developed for low permeability materials. Special care was devoted to the saturation of the specimens that was made under stress conditions close to in-situ, and to conditions ensuring full drainage thanks to a reduced drainage length and low shear rate. Tests were carried out under in-situ, half to in-situ and twice the Terzaghi mean effective in-situ stress at 25°C and 80°C to investigate the effects in the close field of the temperature elevation due to the exothermic nature of the waste. Some radial permeability tests were conducted at various temperatures. The data obtained showed that there is little effect of temperature on the elastic parameters determined, whereas a tendency to a decrease in shear strength was noted, compatible with the few published data. Temperature also appeared to have little effect on the intrinsic permeability, with higher flows mainly due to the decrease in water viscosity.

1. Introduction

In many countries (including Belgium, France and Switzerland), deep argillaceous formations are considered as potential host rock for the disposal of high activity radioactive waste at great depth. Because of low permeability, good self sealing properties and ability to retain radionuclides, the Callovo-Oxfordian (COx) claystone has been selected in France as potential host rock by Andra, the French agency for the management of radioactive waste. Andra developed an Underground Research Laboratory [1] in the COx layer at a depth of 490 m near the village of Bure (East of France) to perform in-situ investigations devoted to various aspects of radioactive waste disposal, including the thermo-hydro-mechanical response of the host rock in the close field, in configurations close to that prevailing during the operational phase of the waste disposal [1].

In the French concept, the canisters containing the radioactive waste are to be placed in disposal cells that consist in horizontal cased microtunnels of 70 cm in diameter and at least 80 m in length. Due to the exothermic nature of radioactive wastes, the rock in the close field and the excavation damaged zone (EDZ) around disposal cells and galleries will be submitted to a temperature elevation. A maximum temperature of 90°C at the cells wall is considered in the French concept, a condition that has obvious economic consequences in terms of both the density of the network of gallery and disposal cells and the number of canisters that can be placed along a given length of excavated disposal cell.

Various investigations have been carried out on the thermal behaviour of clays but that of claystones is much less documented. In clays, the importance of the overconsolidation ratio has clearly been emphasized, with significant effects in volume change and shear strength response [1, 2, 3, 4, 5, 6].

Various investigations have been carried out about the hydro-mechanical behaviour of the COx claystone based on triaxial tests [7, 8, 9, 10, 11]. Actually, published data on the shear strength properties of the COx claystone appear to be somewhat dispersed partly due to the natural variability of the properties of the claystone. The mineralogical composition of the COx claystone changes with depth, in particular in terms of clay and calcite content. The depth of 490 m at which the Bure URL has been excavated corresponds to a maximum clay content of around 50%, selected to ensure the best isolating properties in terms of low permeability, self-sealing and radionuclides retaining ability.

Another possible reason of the observed dispersion of the published mechanical characteristics of the COx is related to the various testing methodologies adopted. A first important parameter is the specimen size that obviously controls the easiness and the period of time necessary to fully saturate specimens. Claystone specimens can be significantly desaturated due to the consecutive effects of coring, core isolation from evaporation, core transportation and storage and, finally, machining in the laboratory. Claystones are very sensitive to changes in water content and triaxial tests carried out at various degrees of saturation evidenced a significant increase of the mechanical strength with lower degree of saturation [8, 9, 12, 13, 14].

Another parameter largely dependent on the specimen size is the quality of the drainage ensured during triaxial testing. Due to the very low permeability of claystones (around 10^{-20} m^2 for the COx claystone), fully drained tests that are necessary for a sound determination of their intrinsic mechanical characteristics are difficult to achieve [15]. Good drainage can be ensured either by adopting slow enough shearing rate or by adopting testing devices with small drainage length. This can be made either by testing

small specimens or by adopting specimen shapes with reduced drainage length [15, 16, 11]. These aspects will be commented in more details later.

In this paper, fully saturated and fully drained triaxial thermal tests were carried out on COx specimens by using a hollow cylinder thermal triaxial device with short drainage length specially developed for low permeability geomaterials [16]. This thermal device has already successfully been used to test the Boom clay from Belgium [17], the Opalinus clay from Switzerland [18] and the COx claystone from France [19]. The experimental program carried out here was aimed at further investigate the effects of temperature on the shear strength response of the COx claystone by comparing tests carried out at 80°C with tests run at 25°C, following the work of Mohajerani et al. [19] on thermal volume changes. Triaxial tests were complemented by constant head radial permeability tests run at both temperatures to investigate the effects of temperature on permeability.

2. The Callovo-Oxfordian claystone

2.1. Mineralogical composition

The COx claystone is a sedimentary rock deposited 155 millions years ago on top of a layer of Dogger limestone that was afterwards covered by an Oxfordian limestone layer. The thickness of the COx layer is about equal to 150 m. The COx claystone is composed of a clay matrix containing some grains quartz and calcite with a mineralogical composition depending on depth with significant changes in carbonate and clay contents. At the depth of the Bure URL (490 m), the average mineralogical composition of COx claystone is as follows [20]: 45-50% clay fraction composed of 10-24% interstratified illite/smectite layers, 17-21% illite, 3-5% kaolinite, 2-3% chlorite. The claystone also contains 28% carbonate, 23% quartz and 4% other minerals (feldspars, pyrite, dolomite, siderite and phosphate minerals). The total porosity varies

in the COx layer between 14% in carbonated levels and 19.5% in the more argillaceous levels [21].

The characteristics of the specimens tested are presented in Table 1. Specimens come from various cores named EST45414 (specimen S1, depth 498 m), EST30734 (S2, depth 612 m) and EST285nn (S3-S4, depth 479 m) and EST45407 (S5, depth 499m). These cores have been extracted at distinct locations. They were selected because they are located approximately at the same level in the claystone layer. Specimen S1 and S5 have a porosity between 13 and 13.5% and a water content around 2.2% corresponding to degrees of saturation between 38 and 39%. A suction of 109 MPa was measured in specimen S1 by using a WP4 dew-point tensiometer. Specimens S2, S3 and S4 have larger porosity between 16.5 and 17.8%, higher water content of around 6% corresponding to degrees of saturation between 80 and 85%. The suctions of specimens S2 and S4 are equal to 31 and 34 MPa, respectively.

2.2. Shear strength and thermal effects in the COx claystone

Published data about the shear properties of the COx claystone determined by running triaxial tests are variable. This is due to the natural variability observed in the COx claystone layer. The specimens tested do not necessarily come from the same borehole location or from the same depth whereas the mineralogical composition of the claystone is dependent upon the depth at which the specimen has been cored. For instance, specimens with higher calcite content and smaller clay content extracted from layers deeper than that of the Bure URL (that is located at the level of maximum clay content) are stiffer and stronger, as recently confirmed in terms of Young modulus by means of micro-indentation and mini compression tests (UCS) run by Hu et al. [22] on COx unsaturated specimens extracted from depths of 490, 503 and 522 m. By testing COx specimens from various depths, Chiarelli [7] showed that the Young modulus increased

with larger calcite content (between 6 and 15 GPa for calcite content between 20 and 52%) and decreased with larger clay fraction (between 15 and 6.5 GPa for clay fraction between 28 and 50%).

Beside natural variability, the testing procedure adopted is another important parameter to consider when comparing the data from various laboratories on COx specimens. Tests have been run in both saturated and unsaturated conditions with drainage conditions not always described in enough detail. By running a series of unconfined compression tests on COx specimens equilibrated at various suctions between 2.7 and 155.2 MPa (by using saturated saline solutions), Pham et al. [13] confirmed the sensitivity of the COx claystone to changes in water content already quoted by Chiarelli et al. [8], Zhang and Rothfuchs [9] and more recently by Zhang et al. [23]. They obtained trends comparable to that evidenced by Valès et al. [12] on the Tournemire shale, with significant increase in strength in drier states. The unconfined compression strengths that Pham et al. [13] obtained at failure varied between 27 MPa in a state close to saturated under a 98% relative humidity (suction 2.7 MPa, water content 5.24%, degree of saturation not given) and 58 MPa in a much drier state under a 32% relative humidity (suction 155.2 MPa, water content 1.65%, degree of saturation not given).

Prior to inspect further experimental data, it was found useful to present the technical procedures used and published in the literature including the depth at which specimens were extracted, the size of the specimen, their porosity, water content, degree of saturation, testing rate and drainage length (an important parameter with respect of drainage conditions). The data obtained in the works of Chiarelli [7] and Chiarelli et al. [8], Zhang and Rothfuchs [9], Pham et al. [13] and Hu et al. [11] are presented in Table 2. One can see that various sizes of triaxial specimens have been

used, the smallest being the 20 × 20 mm cylindrical specimen used by Hu et al. [11], the longest one being the 100 mm high and 35 mm diameter used by Chiarelli [7] and Chiarelli et al. [8]. Pham et al. [13] used a specimen of 72 mm in height and 36 mm in diameter whereas Zhang and Rothfuchs [9] used a slightly larger specimen (40 mm in diameter and 80 mm in length). Both sizes are close to standard triaxial specimens of 38 mm in diameter and 76 mm in height.

Whenever carried out, the saturation procedure has not always been described in details by the authors. Some values of degree of saturation are given, that correspond to the initial one as obtained when receiving the specimen in the laboratory (i.e. between 73 and 100 % for Chiarelli [7] and Chiarelli et al. [8] who tested their specimens at their initial degree of saturation). The smallest degree of saturation was obtained after drying to investigate the effects of change in water content on the shear strength (1.65% by Pham et al. [13] and 2.8% by Zhang and Rothfuchs [9]). Although they did not comment about their saturation procedure, Zhang and Rothfuchs [9] obtained almost fully saturated specimens at S_r = 99%. On their small specimen, Hu et al. [11] achieved complete saturation by imposing a 1.5 MPa back-pressure on the bottom of the specimen until monitoring the same value on the top. The change with time of the pore pressure measured at the top of the specimen indicated that full saturation occurred after 70 hours in the 20 mm high specimen.

The drainage conditions imposed during the tests are not always described in detail. It seems that most often drainage was ensured by porous discs on top and bottom of the specimens. The other important parameter is the strain rate imposed, that varies between the largest value of 6.5×10^{-6} s^{-1} (Zhang and Rothfuchs [9]) in undrained tests down to 10^{-7} s^{-1} in Hu et al [11] in drained tests with a drainage length of 10 mm. The corresponding speeds are also given in Table 2 in μm/mn, knowing that drained tests in

clayey soils (permeability of $10^{-17}m^2$) are typically conducted at a speed of 1 μm/mn with a 19 mm drainage length equal to the specimen radius, thanks to lateral drainage allowed by filter papers placed all around the sample. In this regard, given the claystone average permeability of 10^{-20} m^2, it seems that drainage was not ensured in the tests of the Table run with speeds larger than 3μm/mn and drainage lengths larger than 40 mm. Conversely, the strain rate of 10^{-7} s^{-1} (speed of 0.12 μm/mn) adopted by Hu et al. [11] with a drainage length of 10 mm should ensure satisfactory drainage.

Note that, in fully saturated clayey soil specimens, imperfect drainage leads to over-estimate the shear strength. When specimens are not fully saturated, things are different because water is under a suction state and generally keeps retained by the specimen with only air exchanges. The shear strength properties can then be over-estimated by partial saturation.

Fig. 1 presents a synthesis of the shear strength data from tests of Table 2 from the authors mentioned above, plotted in a diagram giving the shear stress at failure with respect to the constant confining Terzaghi effective stress applied during the test. One observes that the data of Chiarelli [7] at various depths with varying degree of saturation exhibit more dispersion and are located clearly above other data, probably because of partial saturation. The most coherent set of data is provided by Hu et al. [11] on specimens EST30446 from vertical borehole in the URL at a depth of around 521.5 m, with good correspondence between drained and undrained saturated tests. The data of Zhang and Rothfuchs [9] come from both UCS tests and two multistage undrained tests on apparently saturated specimens (saturation procedure not described in the paper). In perfectly saturated clayey soils, undrained triaxial tests carried out at various confining stresses would provide a horizontal failure criterion providing only one value of undrained shear strength. It is not the case here with a slope comparable to that

obtained in drained conditions. Imperfect saturation could be a reason why the criterion is not horizontal. The data of Hu et al. [11] provide, adopting a Mohr Coulomb criterion, a friction angle around 21° close to what could be obtained from that of Zhang and Rothfuchs [9]. The data of Chiarelli [7], [8], more dispersed, would provide higher friction angles.

The cohesion that would be obtained from Zhang and Rothfuchs [9]'s data (9 MPa, Fig. 1) is higher than that from Hu et al. [11], possibly due to partial saturation as well. This is compatible with data on the shear strength properties of unsaturated soils [24] that evidenced little effect of suction on the friction angle but significant effect on the cohesion, the higher the suction, the higher the cohesion.

There is little published data on the thermal behaviour of claystones. In terms of volume changes in clays, the important influence of overconsolidation, initially evidenced by Hueckel and Baldi [2] on Boom clay and Pontida clay, was confirmed by others (see for instance [4] on Boom clay and [5] on compacted clay). It is well established that normally consolidated clays (that never supported any overburden higher than what they supported when extracted) contract when heated under constant load whereas overconsolidated clays (that supported during their geologic history an overburden higher that what they were supporting when extracted, due for instance to erosion of upper layers) tend to exhibit elastic thermal expansion. A combined dilating-contracting behaviour can be observed on slightly overconsolidated clays, like for instance Boom clay.

The volume changes of the COx claystone submitted to temperature elevation under constant isotropic stress close to in-situ conditions was recently investigated in fully saturated and fully drained conditions by Mohajerani et al. [19] by using the hollow cylinder triaxial apparatus. They observed a thermal contraction, evidencing

behaviour comparable to that of normally consolidated clays. On the Opalinus clay, Monfared et al. [18] observed a dilating-contracting behaviour with expansion up to a temperature of 65° close to the maximum estimated temperature supported during its geological history (65-70°C). Expansion was followed by contraction at higher temperature (up to 80°C). Interestingly, a subsequent temperature cycle up to 80°C exhibited thermal expansion, evidencing a thermal hardening phenomenon.

Zhang et al. [25] run at various temperatures (from 20 to 115°C) undrained triaxial shearing tests (strain rate 10^{-7} s^{-1}) under constant 3 MPa confining stress on Opalinus clay specimens with bedding planes inclined of 30-40°. The specimens had an initial degree of saturation of 88%. Zhang et al. [25] observed in such conditions a more ductile behaviour at elevated temperature with clear decrease in strength due to temperature elevation (maximum shear strength of 20 MPa at 20°C and of 5 MPa at 115°C). More recently, Zhang et al. [26] conducted triaxial micro-compression tests on unsaturated standard triaxial specimens submitted to a relative humidity of around 74%. They observed little sensitivity with respect to temperature in the stress strain curves obtained between 20 and 95°C under a confining stress of 15 MPa (around twice the in-situ effective stress), whereas a decrease in peak stress (with small sensitivity in the elastic regime) was observed under a confining stress of 5 MPa (smaller than the in-situ stress). Masri et al. [27] conducted a series of what they called “pseudo-drained” triaxial shear tests at temperatures between 20 and 250°C under three confining pressures (5, 10 and 20 MPa) at an axial strain rate of 10^{-6} s^{-1} on specimens not fully saturated (degree of saturation not provided). Specimens of 37 mm in diameter and 74 mm in height were bored with air pressure from cubic blocks extracted in the Tournemire URL (France). Their observations are comparable to that made by Zhang et al. [25] on Opalinus clay, with significantly more ductile behaviour observed at

elevated temperature and peak stress decreasing from 90 MPa at 20°C down to 40 MPa at 250°C (tests run with bedding perpendicular to specimen axis).

The two previous works indicate that there is a suspicion of having an increase in ductility and a decrease in shear strength in claystones with elevated temperature. However, due to obvious experimental difficulties, these results are based on tests that have not been conducted under fully saturated and drained conditions. The necessity and interest of exploring this issue with well adapted devices and procedures, as proposed in this work, are hence confirmed.

3. Experimental device

3.1 Description

A global overview of the hollow cylinder triaxial cell specially designed to investigate the thermo-hydro-mechanical behaviour of low permeability clays and claystones [16] is presented in Fig. 2a that schematically shows the triaxial cell containing the hollow cylinder specimen (external diameter D_{ext} = 100 mm, internal diameter D_{int} = 60 mm, height H = 70-80 mm). Note that the same confining pressure is applied along both the external and internal lateral faces of the specimen thanks to a connection between these two volumes. As shown in Fig. 2a-b, a major advantage of this device is provided by the two lateral drainages in the inner and outer walls of the hollow cylinder specimen. These drainages are made up of two geotextiles bands placed along the specimen, with no contact between the bands and the upper and lower drainages. These lateral drainages reduce the specimen drainage length down to half the thickness of the hollow cylinder, i.e. 10 mm. Satisfactory drainage conditions are achieved during mechanical and thermal loading provided the strain rate and temperature elevation rate is small enough. Numerical calculations carried out by Monfared et al. [18] showed that a stress

rate of 0.5 kPa/mn ensured satisfactory drainage in hollow cylinder specimens with permeability as low as 10^{-20} m^2.

The axial force is applied by using an integrated piston specially developed (Fig. 2a). The displacements of the piston are controlled by a pressure-volume controller (maximum pressure of 60 MPa) connected to the upper chamber of the piston. The applied axial force is directly measured by a local immersed force sensor fixed at the bottom end of the piston. It can also be estimated from the pressure exerted and measured by the PVC.

Fig. 2b shows a schematic view of the hydraulic connections between the specimen, the pressure-volume controllers (PVC) and the pressure transducers (PT). PVC1 is used to apply the confining pressure whereas the other three PVCs are used to apply and control the pore fluid pressure. The device also comprises a system used to monitor local strains composed of two axial and four radial local displacement transducers (LVDTs, precision ± 1μm, Fig. 2c).

The heating system consists of a heating electric belt placed around the cell with a temperature regulator with a precision of ±0.1°C. Temperature is measured inside the cell close to the specimen by a thermocouple. The cell is covered by insulating layer in order to limit heat exchanges with the environment.

3.2. Preliminary resaturation procedure

As shown by Monfared et al. [16], an interesting feature of the hollow cylinder triaxial cell is its ability to ensure good initial saturation of specimens of very low permeability (around 10^{-20} m^2 in the case of the COx claystone) within a reasonable period of time thanks to a drainage path equal to half the thickness of the hollow cylinder. Proper preliminary resaturation of specimens that have been desaturated during coring, conservation, transport and machining in the laboratory is essential. The

initial degree of saturation of the specimens appears to be an important parameter with respect to specimen quality.

As recalled by Delage et al. [28] on the Boom clay, Monfared et al. [18] on the Opalinus clay and Mohajerani et al. [29] on the COx claystone, it is important to resaturate specimens of swelling clays under stress conditions close to in-situ ones in order to avoid further perturbation due to swelling during hydration. The in-situ state of stress at the level of the Bure URL has been investigated in detail by Wileveau et al. [30] who provided the following values: vertical total stress $\sigma_v = 12.7$ MPa, minor horizontal total stress $\sigma_h = 12.4$ MPa and major horizontal total stress $\sigma_H = 16.2$ MPa, situ pore pressure $u = 4.7$ MPa. Mohajerani et al. [29] used a confining stress of 12 MPa and a pore pressure of 4 MPa, resulting in a Terzaghi effective stress of 8 MPa. So as to reduce the risk of leaks due to possible perforation of the neoprene jacket under high stresses, it was preferred here to adopt the same Terzaghi 8 MPa effective stress value with lower values, i.e. a 9 MPa confining pressure and a 1 MPa pore pressure.

Fig. 3 shows the volume changes calculated from the water injected from the back pressure PVCs compared to that monitored by local LVDT measurements during the saturation phase of tests T3 (specimen EST28514, porosity $\phi = 17.6\%$, initial degree of saturation $S_{ri} = 85\%$) and T6 (specimen EST45407, $\phi = 13.5\%$, $S_{ri} = 39\%$). The curves show that the stabilization of the water injected and of the volume changes derived from the local LVDTs occurred after two days in both cases. The higher volume change obtained from the water injected from the PVC is due to the effect of the water volume needed to saturate the porous elements in contact with the specimen, i.e. the lateral geotextiles and the upper and lower porous discs. One can also observe that the water injected from PVCs in test T6 (7.4%, $S_{ri} = 39\%$, Fig. 3b) is significantly larger than that injected in test T3 (2.3%, $S_{ri} = 85\%$, Fig. 3a) because of the significantly smaller initial

degree of saturation in T6. A slightly larger swelling is monitored by the LVDTs in test T3 (1.18% compared to 1.04% for T6), perhaps linked to the difference in clay fraction between both specimens, with a larger clay fraction in the more porous T3 specimen (porosity 17.6%).

3.3. Radial permeability tests

Steady state permeability measurements were carried out by applying a radial pressure gradient across the specimen and by measuring inflow and outflow fluxes by using the PVCs. Permeability tests were carried out on specimens with an initial backpressure of 1 MPa by closing the valves connected to the top and bottom of the specimen and by applying a pressure excess of 0.5 MPa through the external geotextile while maintaining the internal pressure equal to 1 MPa.

The radial intrinsic permeability k_r (m^2) was calculated using the flow rates as follows:

$$k_r = \frac{Q\mu_w \ln(R_{ext} / R_{\text{int}})}{2\pi h \Delta u} \quad (1)$$

where Q is the water flow; μ_w the water viscosity (equal to 8.90×10^{-4} Pa.s at 25°C and 3.55×10^{-4} Pa.s at 80°C), R_{ext} and R_{int} the external and internal specimen radius, respectively (R_{ext} = 50 mm; R_{int} = 30 mm); h the flow height (h =50 mm); and Δu the pressure difference between the inner and outer walls of the specimen (Δu = 0.5 MPa).

3.4. Comments on the hollow cylinder device

As commented previously, the advantages of the hollow cylinder device in term of both resaturation duration and drainage conditions are provided by the short drainage length equal to half the thickness of the cylinder (10 mm), thanks to the external and internal lateral drainages. Compared to small triaxial specimens that also have short drainage paths, the hollow cylinder configuration also allows the monitoring of axial and radial

local strains thanks to the larger specimen size. Also, this specific configuration allows perform radial permeability tests in sheared specimens by forcing the water flux in the network of shear bands. This ability has proven being quite useful in the investigation of the self-sealing properties of the Boom clay [17] and of the Opalinus clay [31]. However, based on the experience gained in the previous studies during the TIMODAZ European project (see Li et al. [32]) and also gained in previous investigations carried out on the COx clay [19], some difficulties have been met in link with the difficulty of machining 100 mm diameter hollow cylinder specimens (see Monfared et al. [17] for more details). This firstly requires large cores of 100 mm in diameter, which is expensive and not so common. Most cores presently extracted from the Bure URL by Andra have a diameter of 80 mm. In this study, good quality hollow cylinder specimens were obtained on a lathe specially devoted to trimming claystone specimen at CEA, the French research institute in nuclear energy.

For this reason of availability of large diameter cores, the tests of this program had to be carried out on available specimens from different origins and initial characteristics, as shown in Table 1.

3.5. Experimental program

Five different loading paths were performed on six hollow cylinder specimens that were machined with the axis perpendicular to bedding to investigate some aspects of the thermo-hydro-mechanical behaviour of the COx claystone, as described in Table 3 and in Fig. 4. The same stress path was followed for tests T2 and T3. All specimens were previously saturated as described in section 3.2. Tests T1, T2, T3 and T4 were carried out along paths aimed at investigating the shear response at 25°C, as shown in Fig. 4. To do so, constant confining pressure tests were carried out at 25°C close to in-situ

condition (σ_3 = 9 MPa, u = 1 MPa), around half the in-situ condition (σ_3 = 5 MPa, u = 1 MPa) and twice the in-situ condition (σ_3 = 17 MPa, u = 1 MPa).

The same program was planned at 80°C but the test planned under twice the in-situ stress condition failed due to leakage and no more hollow cylinder specimen was available to do it again. The tests under constant confining stress finally performed at 80°C were test T5 on specimen EST45414 (like T1) under stress conditions close to in-situ (σ_3 = 9 MPa, u = 1 MPa) and test T5 on specimen EST 45407 under half the in-situ condition (σ_3 = 5 MPa, u = 1 MPa).

The tests carried out under half the in-situ condition are expected to swell during the stress release from the initial in-situ condition under which they have been resaturated (see Mohajerani et al. [33]). Particular care was put in following this swelling phase to make sure that the specimen reached equilibrium in water content. It seemed that this stress path was preferable to get a relevant response, compared to the standard stress path in which the specimen would have been directly submitted to the desired stress state prior to perform the resaturation procedure.

Steady state permeability tests were also planned in some tests. Their interest is to provide further insight on the effects of temperature, compression and swelling on the permeability. Successful radial steady state permeability tests were performed in test T6 at points B (after resaturation), C (after swelling) and D (after heating the swelled specimen up to 80°C).

4. Experimental results

4.1. Test at 25°C

Test T1, a drained shear test at constant confining stress close to the in-situ effective stress, was carried out with a constant axial displacement rate of 0.4 μm/mn while measuring the strength by using both the immersed force gauge and the pressure

measurement provided by the PVC applying the axial force. One observes in Fig. 5 the changes in axial, radial and volumetric strains with respect to the shear stress ($q = \sigma_1 - \sigma_3$). The curves show that the maximum value of the shear stress at peak is 23 MPa. A good correspondence was observed between the force measured by the immersed force gauge and that obtained from by the external measurement provided by the CPV pressure applied on the piston chamber (not given here). The peak is reached at 0.62% of local axial strain and 0.24% of local radial strain. Note that the two axial LVDTs transducers have not moved at the beginning of the test, up to 4 MPa of shear stress.

Fig. 5 also shows that the axial strain at peak found by external LVDT is of the order of 1.45%, significantly higher than the 0.62% strain monitored by the local axial LVDT. This difference is due to the non-negligible effects of the compressibility of the whole system of axial stress application. It shows that Young's modulus obtained from external axial measurements might be significantly underestimated.

A contracting dilating behaviour is observed before reaching the peak with a transition observed at 16.5 MPa. The post-peak response is controlled by strain localisation and the response of the resulting discontinuity observed after failure. Indeed, one observes on the photographs of the specimen at the end of the test (Fig. 6) a network of shear bands with an inclination of 66° with respect to horizontal. One also notes the darker colour of the specimen due to full saturation, compared to the initial clearer grey colour of COx specimens.

Once resaturated under in-situ stress condition, the specimens of tests T2, T3 and T6 were unloaded to a stress state close to half the in-situ one ($\sigma_3 - u = 4$ MPa) in drained condition with the four drainages connected to a PCV imposing a backpressure $u = 1$ MPa. To do so, the confining pressure was decreased from 9 to 5 MPa at a slow rate of 1 kPa/mn. During this phase, the specimen volume monitored by LVDTs

transducers increased by 1.21%, 1.12% and 0.63% after 12 days for tests T2, T3 and T6 respectively. In a standard fashion, more swelling was observed in the direction perpendicular to bedding as seen in Fig. 7. The larger swelling observed in the specimens of tests T2 and T3 of larger porosity (16.5 and 17.6% respectively) confirm the effect of a larger clay fraction, as previously mentioned in Section 3.2 when describing the resaturation phase.

Specimens were afterwards maintained under a confining pressure of 5 MPa for a few days in order to see possible swelling under a constant mean effective stress lower than the in-situ one (~8 MPa). A volumetric swelling ratio of 0.013%/day, 0.022%/day and 0.010%/day were measured by LVDTs for T2, T3 and T6 respectively.

The specimens of tests T2 (ϕ = 16.5%) and T3 (ϕ = 17.6%) were then sheared under a constant confining stress equal to half the in-situ effective stress (4MPa) in drained conditions with axial displacement rates of 0.5μm/mn and 0.4μm/mn respectively. Fig. 8 shows the axial, radial and volumetric strains changes with respect to shear stress for both specimens. A peak strength value of 10.5 MPa at axial and radial strains of 1.06% and 0.24% respectively is observed for T2. A peak strength value of 10.3 MPa at axial and radial strains of 1.01% and 0.33% respectively was obtained for T3, showing good repeatability in the response of those two specimens of comparable porosity.

Fig. 9 presents the axial, radial and volumetric strain with respect to the shear stress for specimen of test T4 under a constant value of confining stress close to twice the in-situ one (8 MPa) with a peak strength at 25.5 MPa at axial and radial strains of 1.15% and 0.60% respectively.

4.2. Drained heating test

Once resaturated under an effective confining stress close to in-situ (cell pressure $\sigma_3 = 9$ MPa, back pressure $u = 1$ MPa), a drained heating test (T5) was carried out under the same constant effective stress on specimen EST45414 ($\phi = 13\%$). A comparable test (T6) was carried out under half the in-situ effective stresses ($\sigma_3 = 5$ MPa, $u = 1$ MPa) on specimen EST45407 ($\phi = 13.5\%$). To do so, the cell was slowly heated up to 80°C with a slow heating rate of 0.5°C/h [4, 18], keeping the four drainage open (top, bottom, lateral inner and outer).

Fig. 10 presents the thermal local axial, radial and volumetric strains obtained from LVDT measurements during the drained heating test. As already observed by Mohajerani et al. [19], they show that the drained thermal volumetric response of the COx claystone under constant in-situ stress is characterized by a contraction occurring from the beginning of the test, with axial strains slightly larger than radial strains, showing slight degree of anisotropy in the thermal response. This anisotropy shows that the direction perpendicular to bedding (axial strains) is somewhat more sensitive than that parallel to bedding (radial strains). At 80°C, the axial strain is equal to 0.06% (characterised by a slope $C_{T\perp} = 1.14 \times 10^{-5}\,^{\circ}C^{-1}$), compared to 0.06% for the radial strain (characterised by a slope $C_{T\perp} = 1.06 \times 10^{-5}\,^{\circ}C^{-1}$), resulting in a slope of $3.16 \times 10^{-5}\,^{\circ}C^{-1}$ for the volume changes.

Fig. 11 shows the thermal response obtained during the drained heating test carried out under half the in-situ effective stresses (test T6). The changes in axial strain also indicate a continuous and almost linear contraction with a slope (perpendicular to bedding) $C_{T\perp} = 0.96\times 10^{-5}\,^{\circ}C^{-1}$. In this test, no more change was observed in radial strain above 37°C, due to some friction effect in the radial LVDT. However, the changes in axial strain observed up to 37°C are comparable to the radial ones, with a

slope (parallel to bedding) $C_{T\|} = 0.77 \times 10^{-5}$ °C^{-1}. Based on this value, a volumetric thermal contraction coefficient of 2.49×10^{-5} °C^{-1} is obtained. Thermal contraction appears to be slightly smaller under half in-situ stress conditions than under in-situ ones.

4.3. Shear tests at 80°C

Once the drained heating phase completed, specimens of tests T5 and T6 were submitted to drained shearing with a constant axial displacement rate of 0.3μm/min and 0.4μm/min respectively. Fig. 12a shows that the shear stress at 80°C under in-situ stress condition reached a peak value of 20 MPa at 0.75% of axial strain and 0.31% of radial strain in test T5. The volume change is characterized by a contracting behaviour, at the beginning (up to a 14.6 MPa), followed by a dilation phase up to the peak. As previously, Fig. 12a shows that the axial strain found by an external measurement at peak is about 1.2%, significantly higher than that given by the local measurement.

The shear test at 80°C carried out under half the in-situ effective stresses (4MPa) is presented in Fig. 12b. This curves shows that the shear stress reaches its maximum value of 16 MPa at 1.25% and 0.35% of axial and radial strain respectively.

4.4. Failure criterion

All the peak values (q_{max}) obtained in the previous tests are brought together in Fig. 13 together with the data of Hu et al. [11] that also concern fully saturated and drained tests. The tests run at 25°C on three specimens with a porosity of 16-17% are located along a line parallel to that obtained at 80°C on specimens with porosity around 13%. There is unfortunately only one point at 25°C for a specimen with porosity around 13%. The failure points at 80°C obtained under in-situ effective stress from a specimen with porosity close to 13% is located slightly below that at 25°C. This set of data will be further commented in the Discussion section.

4.5. Radial permeability tests

Radial permeability tests were carried out in some cases to investigate the effects of volume changes and of temperature on water transport. Given that specimens were machined with axis perpendicular to bedding, the flow of water during radial permeability tests is governed by the permeability parallel to bedding. As described in Section 3.3, tests were carried out by applying a 1.5 MPa pore pressure on the external lateral face of the hollow cylinder while maintaining the pressure on the internal face equal to the initial back pressure of 1 MPa. The confining pressure was kept equal to 9 MPa.

The inflow and outflow curves monitored by the upstream and downstream PVCs for the test after resaturation under in-situ stress conditions of the specimen of test T6 (porosity 13.6%) are presented in Fig. 14 (in which the Q final inflow and outflow are indicated). Actually, a tiny leak was observed on the upstream PVC when bringing back the pressure from 1.5 to 1 MPa at the end of the test. This leak (estimated by 23% of the monitored inflow at point B) was accounted for and inflow curves corrected accordingly (note however that the correction was made under 1 MPa whereas tests were carried out under 1.5 MPa). Less confidence is hence given to inflow curves compared to outflow curve that were not affected by any leak.

Fig. 14 shows that, once the upstream injection starts, it was necessary to wait for 30 minutes before monitoring any outflow with the downstream PVC. This period of time was necessary to install steady state conditions and to reach the new effective stress state resulting from the 1.5 MPa pore pressure exerted along the external face of the specimen. By applying Darcy's law on the outflow observed at the end of test ($Q = 3.35 \times 10^{-12}$ m^3/s), a radial permeability of 0.9×10^{-20} m^2 is obtained. That obtained from the inflow value ($Q = 3.88 \times 10^{-12}$ m^3/s) is close, although slightly larger

($k = 1.1 \times 10^{-20}$ m^2), confirming the good quality of the measurement (with satisfactory correction of the upstream leak).

Fig. 14b shows the changes in volume obtained from water exchanges (calculated from the upstream and downstream PVCs data) and from local LVDTs measurements. For some reason, the two curves are not in good correspondence during the first 14 hours with LVDTs indicating fast swelling during the first two hours. Both curves afterwards correspond and indicate that the specimen slightly swells (0.034% after 27 hours with a final swelling rate of 4.3×10^{-4} h^{-1}). The amount of water adsorbed during the test explains the slight difference between the inflow and outflow data, and between the two calculated permeabilities.

Another radial permeability test was carried out in test T6 after releasing the confining stress to half the in-situ value to investigate the effect of the resulting 0.63% swelling (Point C, Fig. 4). Inflow and outflow data (Fig. 15a) are comparable to that observed above with no outflow during the first hour, providing at the end of test radial permeability values of 1.2×10^{-20} m^2 and 1.6×10^{-20} m^2, respectively. These values are slightly higher than before stress release and are related to the 0.63% swelling. The PVC volume change curve (Fig. 15b) provides a slightly larger volume change value than LVDTs at end of test. The final swelling rate is 5.9×10^{-4} h^{-1}.

The data of the permeability test finally carried out after drained heating (Point D, Fig. 4, test T6, thermal contraction 0.106%, see Fig. 11) are presented in Fig. 16 a and b. This test had to be stopped after only 7 hours with a final swelling rate of 3.7×10^{-3} h^{-1}. Even after a shorter period of time, swelling is close to 0.07%, i.e. almost twice that observed in the two previous tests at 25°C, indicating possible enhancing of swelling with elevated temperature. Compared to previous tests at 25°C, larger fluxes are obtained ($Q_{inflow} = 2.52 \times 10^{-11}$ m^3/s and $Q_{outflow} = 1.58 \times 10^{-11}$ m^3/s). Here, the

difference between inflow and outflow is larger than previously. Given that the upstream leak correction done at 25°C could not be valid here, only the outflow curve is considered to provide an (intrinsic) permeability value equal to 1.8×10^{-20} m^2. As further commented in the Discussion session, larger fluxes are related to the decrease in water viscosity. A larger permeability is observed at 80°C in spite of a slight porosity reduction.

4. Discussion

4.1 Elastic response

A series of triaxial tests have been conducted on COx claystone specimens along various thermo-hydro-mechanical paths (Fig. 4) in fully saturated and drained conditions by using the hollow cylinder device. Although all of the tests initially planned were not successful because of the technical difficulty of getting hollow cylinder specimens and of running hollow cylinder triaxial tests, some conclusions can be drawn from the data obtained.

The various shear stress/axial strain curves obtained on specimens trimmed with axis perpendicular to bedding allow the determination of some elastic constants that partly describe the transverse isotropic elastic behaviour of the COx claystone. As described by Cheng et al. [34], the stress-strain elastic relationship for a transverse isotropic material is as follows:

$$\begin{pmatrix} d\varepsilon_1 \\ d\varepsilon_2 \\ d\varepsilon_3 \end{pmatrix} = \begin{pmatrix} \frac{1}{E_1} & -\frac{\nu_{21}}{E_2} & -\frac{\nu_{21}}{E_2} \\ -\frac{\nu_{12}}{E_1} & \frac{1}{E_2} & -\frac{\nu_{23}}{E_2} \\ -\frac{\nu_{12}}{E_1} & -\frac{\nu_{23}}{E_2} & \frac{1}{E_2} \end{pmatrix} \begin{pmatrix} d\sigma_1 \\ d\sigma_2 = 0 \\ d\sigma_3 = 0 \end{pmatrix} \quad (2)$$

with $d\sigma_2 = d\sigma_3 = 0$ under "triaxial" conditions and where ν_{23} and E_2 are the Poisson ratios and Young modulus in the plane of isotropy (2-3), and ν_{12}, ν_{21} and E_1 are the

Poisson ratio and Young modulus in the plane perpendicular to the plane of isotropy. The Young modulus and Poisson ratio perpendicular to bedding can be calculated by using the data of the drained triaxial test using Eq. (3) and Eq. (4).

$$\frac{d\varepsilon_1}{d\sigma_1} = \frac{1}{E_1} \quad (3)$$

$$\frac{d\varepsilon_2}{d\sigma_1} = -\frac{\nu_{12}}{E_1} \quad (4)$$

From the data of Fig. 5 under a confining stress close to in-situ (8 MPa Terzaghi effective stress), a value E_1 = 3.2 GPa is obtained from the shear stress-axial strain curve for a mobilisation of 0.1% of axial strain, with ν_{12} = 0.30 (Table 4). When the confining stress has been released close to half the in-situ one, values E_1 = 1.5 GPa and 1.3 GPa are deduced from tests T2 and T3 respectively with Poisson's ratio ν_{12} = 0.10 in both cases (Fig. 8). Conversely, when the confining stress is increased to twice the in-situ stress (test T4, Fig. 9), values of Young modulus and Poisson's ratio of 5.5 GPa and 0.34, respectively, are obtained.

At 80°C, the estimated values of the E_1 Young's modulus and the ν_{12} Poisson ratio are E_1 = 3.4 GPa and ν_{12} = 0.26, respectively, under a confining stress close to in-situ. Values E_1 = 1.4 GPa and ν_{12} = 0.10, respectively, were obtained under a confinement of half the in-situ stress.

All the values obtained at 25 and 80°C are plotted together in Fig. 17 that clearly shows that there is no effect of temperature on the elastic properties determined here (Young's modulus E_1 and Poisson coefficient ν_{12}). Similar comparison has been drawn by Mohajerani et al. [19] from isotropic compression tests, showing no effect of temperature (80°C) on the elastic compression parameters. The Young's modulus also regularly increases with the effective confining stress. It is important to recall that all

the points tested here started from previous saturation under in-situ stress, with the smaller confining stress at half in-situ stress (4 MPa) obtained by subsequent stress release (and mobilisation of swelling). The Poisson ratio ν_{12}, equal to 0.30 at initial state under in-situ stress (8 MPa) decreases to 0.10 when the confining effective stress is released at 4 MPa, both at 25 and 80°C, confirming the independency of the elastic parameters with respect to temperature. Conversely, ν_{12} only slightly changes from 0.30 to 0.34 when the confining effective stress is increased at 16 MPa. This could indicate that the decrease observed when releasing the effective confining stress could be related to the slight swelling mobilized, an hypothesis to further confirm.

It seems difficult to compare the data obtained here with published data that appear to have generally been obtained based on other experimental procedure like for instance, for the Young modulus, from unconfined compression tests under not fully saturated conditions [13, 26]. Data on the Poisson ratio are less available.

4.2 Thermal volume changes

Two drained heating tests were performed to investigate the thermal volumetric response of the COx claystone under stress conditions close to in-situ (mean Terzaghi effective stress of 8 MPa) and to half the in-situ stress (mean Terzaghi effective stress of 4 MPa). They confirmed the contracting behaviour already evidenced by Mohajerani et al. [19], but with smaller contraction coefficient, as indicated in Table 5. Whereas Mohajerani et al. [19] observed a significantly anisotropic thermal response with thermal contraction coefficients of 3.15 and 6.50×10^{-5}°C^{-1} parallel and perpendicular to bedding, respectively, the contraction observed here is less marked and less anisotropic with $C_{T\perp} = 1.15 \times 10^{-5}$°C^{-1} perpendicular to bedding and $C_{T//} = 1.06 \times 10^{-5}$ °C^{-1} parallel to bedding under in-situ stress. These values slightly decreased to $C_{T\perp} = 0.96 \times 10^{-5}$°C^{-1} and $C_{T//} = 0.77 \times 10^{-5}$°C^{-1} under half in-situ stress. This smaller

contraction under smaller stress is not surprising. A possible reason of the significantly smaller contraction observed here could come from the differences in origin and in porosity between the specimens, with Mohajerani et al.'s [19] specimen significantly more porous (17.9% compared to around 13% here). More porous samples have larger clay content and clay content is the driving force of thermal contraction, given that the grains of quartz and calcite contained in the clay matrix simultaneously expand, probably resulting in some thermal damage at the interface between the grains and the clay matrix.

The COx claystone is known to have supported a maximum temperature of 50°C during its geological history [35]. Unlike what was observed in the Opalinus clay by Monfared et al. [18], one does not observe here an initial thermal expansion up to 50°C. For some reason, the thermal hardening phenomenon observed on the Opalinus clay is not observed here.

4.3 Shear strength and temperature effects

Fig. 13 shows the values of peak strength ($q_{\max}$) as a function of effective mean stress p' for all of the tests carried out here, together with the data obtained by Hu et al. [11] at 25°C under fully saturated conditions. The porosity of the specimens is also mentioned, given that the specimens tested by Hu et al. [11] have a porosity of around 13%. The Figure shows that the failure shear stress at 25°C are reasonably well organised with respect to their porosity, with good correspondence between tests T1 (EST45414) under in-situ confining stress (T = 25°C, p' = 8 MPa, ϕ = 13%, $q_{failure}$ = 23 MPa) and the data obtained by Hu et al. [11] at a comparable value of porosity and same temperature. The failure data obtained at 25°C with the specimens of 17% porosity are located below that at 13%, exhibiting smaller shear strength for more porous specimens, in a standard fashion. All tests at 25°C (including Hu et al. [11] data)

are aligned along parallel lines that define a friction angle of 21° equal to that proposed by Hu et al. [11]. There is a decrease in cohesion that makes the more porous specimen weaker with a cohesion of 1.94 MPa at 17% compared to 4.2 MPa at 13%. Note however that the shear strength data obtained here appear to be somewhat small with respect to the data of undrained compression tests carried out for Andra by various laboratories that provided undrained compression strengths (UCS) around 20 MPa (Conil, personal communication). Indeed, Pham et al. [13] reported a UCS of 28 MPa on a specimen not fully saturated tested under a 98% relative humidity. A possibility of underestimating the shear strength by the size and shape of the specimens tested (hollow cylinder here and small cylinder for Hu et al. [11]) might be considered.

The two points obtained at a porosity of 13% at a temperature of 80°C are located slightly below the points at the same porosity and 25°C, indicating a slight reduction in shear strength due to temperature. The slight difference observed is actually in the range of the dispersion observed when testing COx specimens, and this preliminary observation is of course to be confirmed by further fully saturated and drained tests. This trend is however in agreement with previous suggestions taken from the works of Zhang et al. [25] on the Opalinus clay and of Masri et al. [27] on the Tournemire shale.

4.4 Permeability tests

Steady state radial permeability tests were performed by imposing a pore pressure increase ($\Delta u = 0.5$ MPa) on the outer face while maintaining the pore pressure equal to 1 MPa on the inner face of the hollow specimen. Water exchanges were monitored by using the PVCs and LVDTs were used to monitor local volume changes. In spite of some differences observed in the transient phase during the set up of the new effective stress conditions resulting from the application of the 1.5 MPa external pore pressure,

the comparison of volume change data from LVDT measurements and from the water exchanges monitored by the PVCs was reasonably satisfactory (in spite of a tiny leak), providing some confidence in the permeability values obtained.

The radial permeability values (parallel to bedding) obtained at various stages of test T6 (points B, C and D in Fig. 4) are presented in Table 6. The values of permeability adopted and discussed below are that obtained from the outflow curves. A reference permeability value of 0.9×10^{-20} m^2 was obtained under in-situ stress conditions, a value in the range of magnitude of published data (more often measured along the axial direction) for the COx claystone, between 10^{-20} and 10^{-22} m^2 m^2 [33, 36, 37, 38].

A slight change from 0.9×10^{-20} m^2 to 1.2×10^{-20} m^2 was obtained after the 0.63% swelling due to stress release from in-situ to half the in-situ stress. After drained heating at 80°C (with a thermal contraction of 0.12% followed by a swelling of 0.07%), larger inflow and outflow were observed due to the increase in water viscosity (from 8.90×10^{-4} Pa.s at 25°C to 3.55×10^{-4} Pa.s at 80°C). The permeability at 80°C appeared to be slightly larger and equal to 1.8×10^{-20} m^2. Although these first results should be confirmed, they show that the permeability is not totally independent of temperature, unlike what was previously observed on the Boom clay [39], with a slight increase with temperature. Note that this tests also showed an enhancement of swelling with temperature, with around twice more swelling at 80°C compared to 25°C under same stress conditions.

5. Conclusion

Published data on the shear strength properties of the Callovo-Oxfordian claystone exhibit some variability due to the natural variability of the deposit, to the changes of the claystone characteristics with depth and also to the testing procedures adopted. An inspection of published data indeed showed that the specimens tested came from various boreholes and from various depths and that the testing procedures were variable in terms of specimen saturation and drainage conditions. It is well known that partial saturation and drainage overestimate the shear strength properties of the COx claystone, and this seems to be somewhat linked to the variability observed in the published data.

Few data are available about the thermal response of the COx claystone. The tests carried out here were performed after careful saturation under in-situ stress conditions and in fully drained conditions thanks to the use of a hollow cylinder triaxial apparatus with reduced drainage length specially designed for testing low permeability rocks. Triaxial tests were carried out at 25 and 80°C to get some preliminary insights on the effects of temperature on the shear strength properties of the claystone. Also, some steady state radial permeability tests were carried out at 25 and 80°C to investigate the effect of temperature on the claystone permeability.

Although somewhat small with respect to the previous UCS data gathered by Andra, the shear strength data obtained here are in good agreement with that of tests also carried out in fully saturated and drained conditions by Hu et al. [11] on specimens of the same porosity (13%). Some effects of the porosity have also been evidenced, with smaller shear strength values obtained on specimens with higher porosity (17%). The thermal contraction of the COx claystone upon heating under constant in-situ stress evidenced by Mohajerani et al. [19] was confirmed. Subsequent shear tests at 80°C

showed little changes of the elastic parameters with temperature, confirming the findings of Mohajerani et al. [19]. The preliminary results obtained in this work evidenced a more ductile response and slightly smaller shear strengths of the COx claystone at elevated temperature, in agreement with the few available published data on shales and claystones. Finally, radial permeability tests performed parallel to bedding demonstrated that the intrinsic permeability did not change significantly with elevated temperature, the larger flow observed at 80°C during the test being mainly due to the decrease in viscosity of water.

The preliminary data obtained here on temperature effects on the shear strength behaviour of the COx claystone need to be further confirmed by complementary tests, they however confirm some trends already observed on the COx claystone and on other clay rocks. A better understanding of the thermo-hydro-mechanical response of claystone will allow a better understanding and modelling of the coupled THM actions that prevail in the close field once the exothermic wastes have been placed.

6. Acknowledgements

The authors are grateful to Andra who founded this work that is part of the PhD work of the first author. Andra also provided the COx specimens tested in this work.

7. References

[1] ANDRA (2005). Synthesis argile: evaluation of the feasibility of a geological repository in argillaceous formation. http://www.andra.fr/international/download/andra-international-en/document/editions/266va.pdf

[2] Hueckel T, Baldi G. Thermoplasticity of saturated clays: experimental constitutive study. Journal of Geotechnical Engineering 1990; 116(12):1768–1796.

[3] Hueckel T, Pellegrini R. Thermoplastic modeling of undrained failure of saturated clay due to heating. Soils Found 1991; 31(3):1-16.

[4] Sultan N, Delage P, Cui YJ. Temperature effects on the volume change behaviour of Boom clay. Engineering Geology 2002; 64(2-3):135-145.

[5] Cekerevac C, Laloui L. Experimental study of thermal effects on the mechanical behaviour of a clay. International Journal for Numerical and Analytical Methods in Geomechanics 2004; 28:209–228.

[6] Hueckel T, François B, Laloui L. Explaining thermal failure in saturated clays. Géotechnique 2009; 59 (3):197-212.

[7] Chiarelli AS. Étude expérimentale et modélisation du comportement mécanique de l'argilite de l'est. PhD thesis, Université Lille I ; 2000.

[8] Chiarelli AS, Shao JF, Hoteit N. Modeling of elastoplastic damage behavior of a claystone. International Journal of Plasticity 2003; 19:23-45.

[9] Zhang CL, Rothfuchs T. Experimental study of the hydro-mechanical behaviour of the Callovo-Oxfordian argillite. Applied Clay Science 2004; 26(1-4): 325-336.

[10] Hoxha D, Giraud A, Homand F, Auvray C. Saturated and unsaturated behaviour modelling of Meuse-Haute/Marne argillite. International Journal of Plasticity 2007; 23:733–766.

[11] Hu DW, Zhang F, Shao JF. Experimental study of poromechanical behavior of saturated claystone under triaxial compression. Acta Geotechnica 2014a; 9:207-214.

[12] Valès F, Nguyen Minh D, Gharbi H, Rejeb A. Experimental study of the influence of the degree of saturation on physical and mechanical properties in Tournemire shale (France). Applied Clay Science 2004; 26:197–207.

[13] Pham QT, Vales F, Malinsky L, Nguyen Minh D, Gharbi H. Effects of desaturation-resaturation on mudstone. Physics and Chemistry of the Earth 2007; 32:646–655.

[14] Yang D, Chanchole S, Valli P, Chen L. Study of the Anisotropic Properties of Argillite Under Moisture and Mechanical Loads. Rock Mechanics and Rock Engineering 2012; 46(2):247–257.

[15] Wu B, Tan CP, Aoki T. Specially designed techniques for conducting consolidated undrained triaxial tests on low permeability shales. International Journal of Rock Mechanics and Mining Sciences 1997; 34:3-4), paper No. 336.

[16] Monfared M, Delage P, Sulem J, Mohajerani M, Tang AM, De Laure E. A new hollow cylinder triaxial cell to study the behaviour of geomaterials with low permeability. International Journal of Rock Mechanics and Mining Sciences 2011; 48 (4):637-649.

[17] Monfared M, Sulem J, Delage P, Mohajerani M. On the THM behaviour of a sheared Boom clay sample: Application to the behaviour and sealing properties of the EDZ. Engineering Geology 2012; 124:47-58.

[18] Monfared M, Sulem J, Delage P, Mohajerani M. A laboratory investigation on thermal properties of the Opalinus claystone. International Journal of Rock Mechanics and Rock Engineering 2011b; 44(6):735-747.

[19] Mohajerani M, Delage P, Sulem J, Monfared M, Tang A.M, Gatmiri B. The thermal volume change of the Callovo-Oxfordian claystone. International Journal of Rock Mechanics and Rock Engineering 2014; 47:131-142.

[20] Gaucher G, Robelin C, Matray JM, Négrel G, Gros Y, Heitz JF, Vinsot A, Rebours H, Cassagnabère, Bouchet A. ANDRA underground research laboratory: interpretation of the mineralogical and geochemical data acquired in the Callovian-Oxfordian formation by investigative drilling. Physics and Chemistry of the Earth 2004; 29:55-77.

[21] Yven B, Sammartino S, Geroud Y, Homand F, Villieras F. Mineralogy, texture and porosity of Callovo-Oxfordian claystones of the Meuse/Haute-Marne region (eastern Paris Basin). Mémoires de la Société géologique de France, ISSN 0249-7549 2007; 178: 73-90.

[22] Hu DW, Zhang F, Shao JF, Gatmiri B. Influences of Mineralogy and Water Content on the Mechanical Properties of Argillite. Rock Mechanics and Rock Engineering 2014b; 47:157-166.

[23] Zhang F, Xie SY, Hu DW, Shao JF, Gatmiri B. Effect of water content and structural anisotropy on mechanical property of claystone. Applied Clay Science 2012; 69:79–86.

[24] Fredlund DG, Rahardjo H, Fredlund MD. Unsaturated soil mechanics in engineering practice. 2012; Wiley, New-York.

[25] Zhang CL, Rothfuchs T, Su K, Hoteit N. Experimental study of the thermo-hydro-mechanical behaviour of indurated clays. Phys Chem Earth Parts A/B/C 2007; 32(8–14):957–965.

[26] Zhang F, Hu DW, Xie SY, Shao JF. Influences of temperature and water content on mechanical property of argillite. European Journal of Environmental and Civil

Engineering 2014; 18(2):173–189.

[27] Masri M, Sibai M, Shao JF, Mainguy M. Experimental investigation of the effect of temperature on the mechanical behavior of Tournemire shale. International Journal of Rock Mechanics and Mining Sciences 2014; 70:185–191.

[28] Delage P, Le TT, Tang AM, Cui YJ, Li XL. Suction effects in deep Boom clay block specimens. Géotechnique 2007; 57(1):239–244.

[29] Mohajerani M, Delage P, Monfared M, Tang A.M, Sulem J, Gatmiri B. A laboratory investigation of thermally induced pore pressures in the Callovo-Oxfordian claystone. International Journal of Rock Mechanics and Mining Sciences 2012; 52:112-121.

[30] Wileveau Y, Cornet FH, Desroches J, Blumling P. Complete in situ stressdetermination in an argillite sedimentary formation. Phys Chem Earth A/B/C 2007; 32(8–14):866–78.

[31] Monfared M, Sulem J, Delage P, Mohajerani M. Temperature and Damage Impact on the Permeability of Opalinus Clay. International Journal of Rock Mechanics and Rock Engineering 2014; 47:101–110.

[32] Li Y, Weetjens E, Sillen X, Vietor T, Li X, Delage P, Labiouse V, Charlier R. Consequences of the thermal transient on the evolution of the damaged zone around a repository for heat-emitting high-level radioactive waste in a clay formation: a performance assessment perspective. Rock Mechanics and Rock Engineering 2014; 47:3-19.

[33] Mohajerani M, Delage P, Monfared M, Tang A.M, Sulem J, Gatmiri B. Oedometric compression and swelling behaviour of the Callovo-Oxfordian argillite. International Journal of Rock Mechanics and Mining Sciences 2011; 48(4):606-615.

[34] Cheng A HD. Material coefficients of anisotropic poroelasticity. International Journal of Rock Mechanics and Mining Sciences 1997; 34(2):199-205.

[35] Blaise T, Barbarand J, Kars M, Ploquin F et al. Reconstruction of low temperature (<100 _C) burial in sedimentary basins: A comparison of geothermometer in the intracontinental Paris Basin. Marine and Petroleum Geology 2013; **http://dx.doi.org/10.1016/j.marpetgeo.2013.08.019**.

[36] Escoffier S. Caractérisation expériementale du comportement hydro-mécanique des argillites de Meuse/ Haute Marne. PhD thesis, INPL Nancy ; 2002.

[37] Escoffier S, Homand F, Giraud A, Hoteit N, Su K. Under stress permeability determination of the Meuse/Haute-Marne mudstone. Engineering Geology 2005; 81:329–340.

[38] Delay J, Trouiller A, Lavanchy JM. Propriétés hydrodynamiques du Callovo-Oxfordien dans l'Est du bassin de Paris : comparaison des résultats obtenus selon différentes approches 2006 ; C.R. Geoscience 338.

[39] Delage P, Sultan N, Cui YJ. On the thermal consolidation of Boom clay. Canadian Geotechnical Journal 2000; 37(2):343-354.

Tables

Figures

Fig. 1. Published shear strength data of the COx claystone.

Fig. 2. (a): Hollow cylinder triaxial cell, (b): Scheme of the hydraulic connections, (c): Local strain measurement system.

Fig. 3. Volume changes and water exchanges during resaturation phase, (a): test T3, (b): test T6.

Fig. 4. Thermo-hydro-mechanical paths followed during the tests carried out.

Fig. 5. Drained shear test under in-situ effective stresses at 25°C, test T1.

Fig. 6. COx claystone at the end of the test T1.

Fig. 7. Drained isotropic unloading phase, (a): T2, (b): T3, (c): T6.

Fig. 8. Drained shear test under half in-situ effective stresses at 25°C, (a): test T2, (b): test T3.

Fig. 9. Drained shear test under twice in-situ effective stresses at 25°C, test T4.

Fig. 10. Axial, radial and volumetric strains measured during a drained heating test (0.5°C/h) under in-situ effective stresses, test T5.

Fig. 11. Axial, radial and volumetric strains measured during a drained heating under half in-situ effective stresses, test T6.

Fig. 12. Drained shear test at 80°C, (a): test T5, (b): test T6.

Fig. 13. Shear strength of all tests carried out in the plan q-p'.

Fig. 14. Radial permeability test at point B, after resaturation T6, (a): inflow and outflow, (b): volume change.

Fig. 15. Radial permeability test at point C, after swelling T6, (a): inflow and outflow, (b): volume change.

Fig. 16. Radial permeability test at point D, after heating T6, (a): inflow and outflow, (b): volume change.

Fig. 17. Elastic parameters, (a): Young's modulus, (b): Poisson coefficient.

Table 1

Table 1. Initial characteristics of the tested specimens.

Specimen	Ref. Core	Depth (m)	Height (mm)	Water content (%)	Dry unit mass (Mg/m^3)	Porosity (%)	Degree of saturation (%)	Suction (MPa)
S1	EST45414	498	73.13	2.11	2.35	13.0	38	109
S2	EST30734	612	73.95	5.88	2.26	16.5	80	31
S3	EST28514	477	75.00	6.76	2.21	17.6	85	
S4	EST28518	479	71.02	6.10	2.20	17.8	80	34
S5	EST45407	499	72.60	2.27	2.34	13.5	39	

Table 2

Table 2. Characteristics published tests about the shear properties of the COx claystone.

Authors	N° Specimen	Depth (m)	Spec. height (mm)	Spec. diameter (mm)	Porosity (%)	Water content (%)	Degree of saturation (%)	Type of test	Testing rate (s^{-1}) μm/mn Drainage length H
Chiarelli (2000), Chiarelli et al. (2003)	EST 02172	451-467	100	35	11.5* *Est. 15.3*	4 – 5.7	73 – 93	Triaxial	6×10^{-6} 3.6μm/mn H = 50 mm
Chiarelli (2000), Chiarelli et al. (2003)	EST 02277	469	100	35	11 – 13.5* *Est. 14.6 – 18*	4 – 7	85 – 100	Triaxial	6×10^{-6} 3.6μm/mn H = 50 mm
Chiarelli (2000), Chiarelli et al. (2003)	EST 02354	482	100	35	11.8 – 13.8* *Est. 15.7 – 18.4*	4 – 7	90 – 100	Triaxial	6×10^{-6} 3.6μm/mn H = 50 mm
Zhang & Rothfuchs (2004)	EST 05677-02	487	80	40	16.1	7.1	99	UCS	6.5×10^{-6} 3.1μm/mn H = 40 mm
Zhang & Rothfuchs (2004)	EST 05677-04	487	80	40	16.1	2.8	39	UCS	6.5×10^{-6} 3.1μm/mn H =40 mm
Zhang & Rothfuchs (2004)	EST 05677-01	487	98	50	16.1	7.1	99	Undrained triaxial multistage	6.5×10^{-6} 3.8μm/mn H =49 mm
Pham et al. (2007)	EST 205D	451	72	36	10 – 14	1.65 – 5.24	Various S_r	UCS	Not given
(2014a)	EST 30446	521.5	20	20	11.8	6.2	100	Triaxial	10^{-7} s^{-1} 0.12μm/mn H = 10 mm

* porosity value obtained by Chiarelli et al. (2003) from mercury intrusion porosimetry tests. Estimated total porosity values are given in italics based on our observation that 25% of the total porosity was not intruded at 200 MPa in the tests that we performed on COx specimens at 490 m.

Table 3

Table 3. Experimental programme.

Test	Specimen	Ref. Core	Programme	Permeability test
T1	S1	EST45414	Shear under σ' = 8MPa at 25°C [B-C]	-
T2	S2	EST30734	Isotropic unloading to σ' = 4MPa (swelling) [B-C], shear at 25°C [C-D]	-
T3	S3	EST28514	Isotropic unloading to σ' = 4MPa (swelling) [B-C], shear at 25°C [C-D]	-
T4	S4	EST28518	Drained isotropic compression up to σ' = 16MPa [B-C], shear at 25°C [C-D]	-
T5	S1	EST45414	Drained heating up to 80°C [B-C], shear under σ' = 8MPa at 80°C [C-D]	-
T6	S5	EST45407	Isotropic unloading to σ' = 4MPa [B-C], drained heating up to 80°C [B-C], shear at 80°C [C-D]	[B], [C], [D]

Table 4

Table 4. Evolution of the elastic parameters.

Test	Ref. Core	Porosity (%)	σ' (MPa)	Temperature (°C)	q_{max} (MPa)	E_1 (GPa)	ν_{12}
T1	EST45414	13.0	8	25	23.1	3.2	0.30
T2	EST30734	16.5	4	25	10.5	1.5	0.10
T3	EST28514	17.6	4	25	10.3	1.3	0.10
T4	EST28518	17.8	16	25	24.6	5.5	0.34
T5	EST45414	13.0	8	80	20.0	3.4	0.26
T6	EST45407	13.5	4	80	16.1	1.4	0.10

Table 5

Table 5. Thermal contraction coefficients.

Specimen	Ref. Core	σ' (MPa)	Depth (m)	Porosity (%)	$C_{T//}$ (x 10^{-5} °C^{-1})	$C_{T\perp}$ (x 10^{-5} °C^{-1})
S5	EST45414	8	491	13.0	1.06	1.15
S6	EST45407	4	491	13.5	0.77	0.96
Mohajerani et al. (2014)	EST25820	8	480	17.9	3.15	6.50

Table 6

Table 6. Effect of swelling and temperature on the COx claystone permeability (T6, porosity 13.5 %).

State	Test	Ref. Core	$k_{r\ inflow}$ (m^2)	$k_{r\ outflow}$ (m^2)
After resaturation, 25°C, [B]	T6	EST45407	1.1×10^{-20}	0.9×10^{-20}
After swelling, 25°C, [C]	T6	EST45407	1.6×10^{-20}	1.4×10^{-20}
After heating, 80°C, [D]	T6	EST45407	2.9×10^{-20}	1.8×10^{-20}

Figure 1

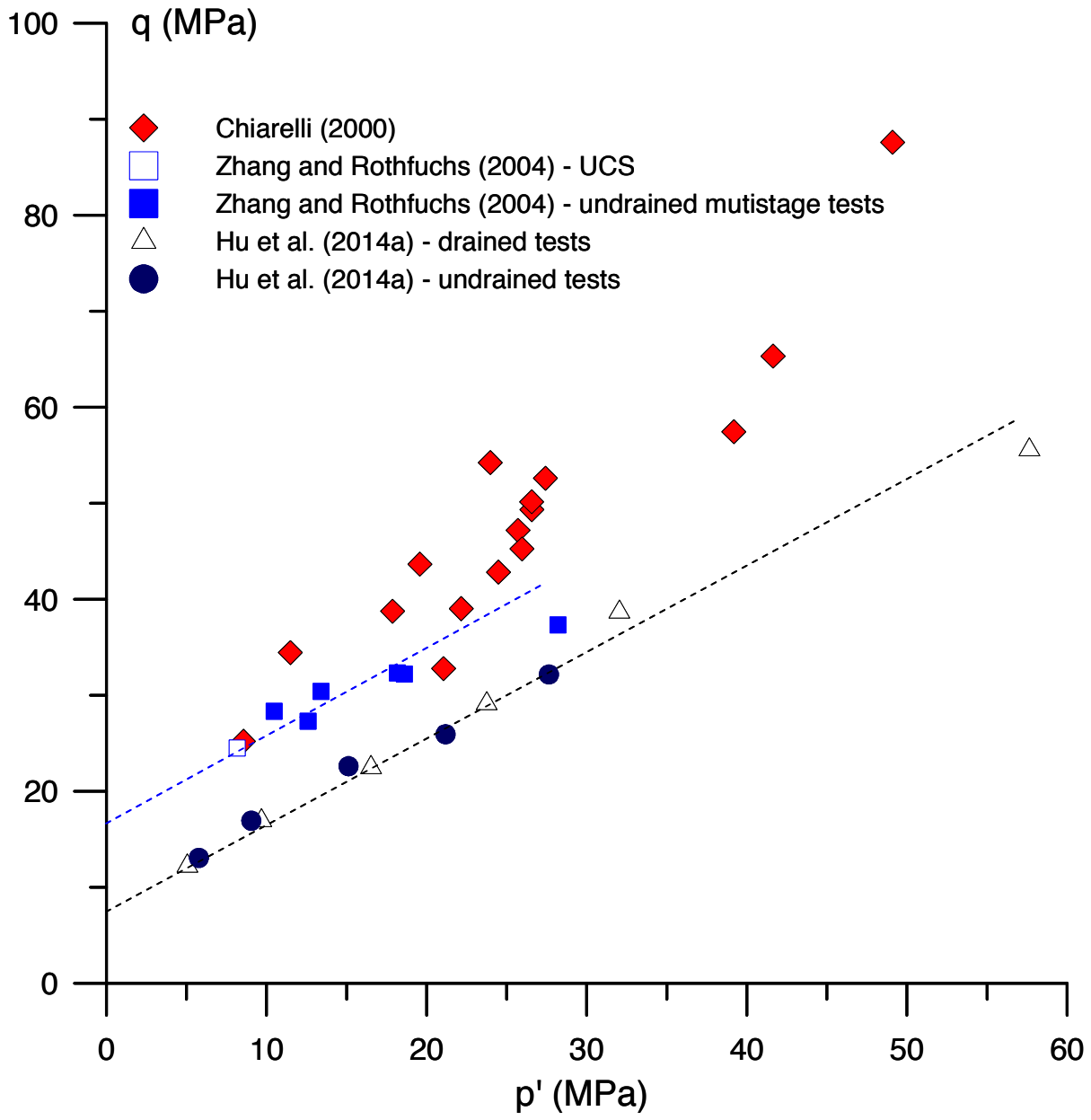

Fig. 1. Published shear strength data of the COx claystone.

Figure 2

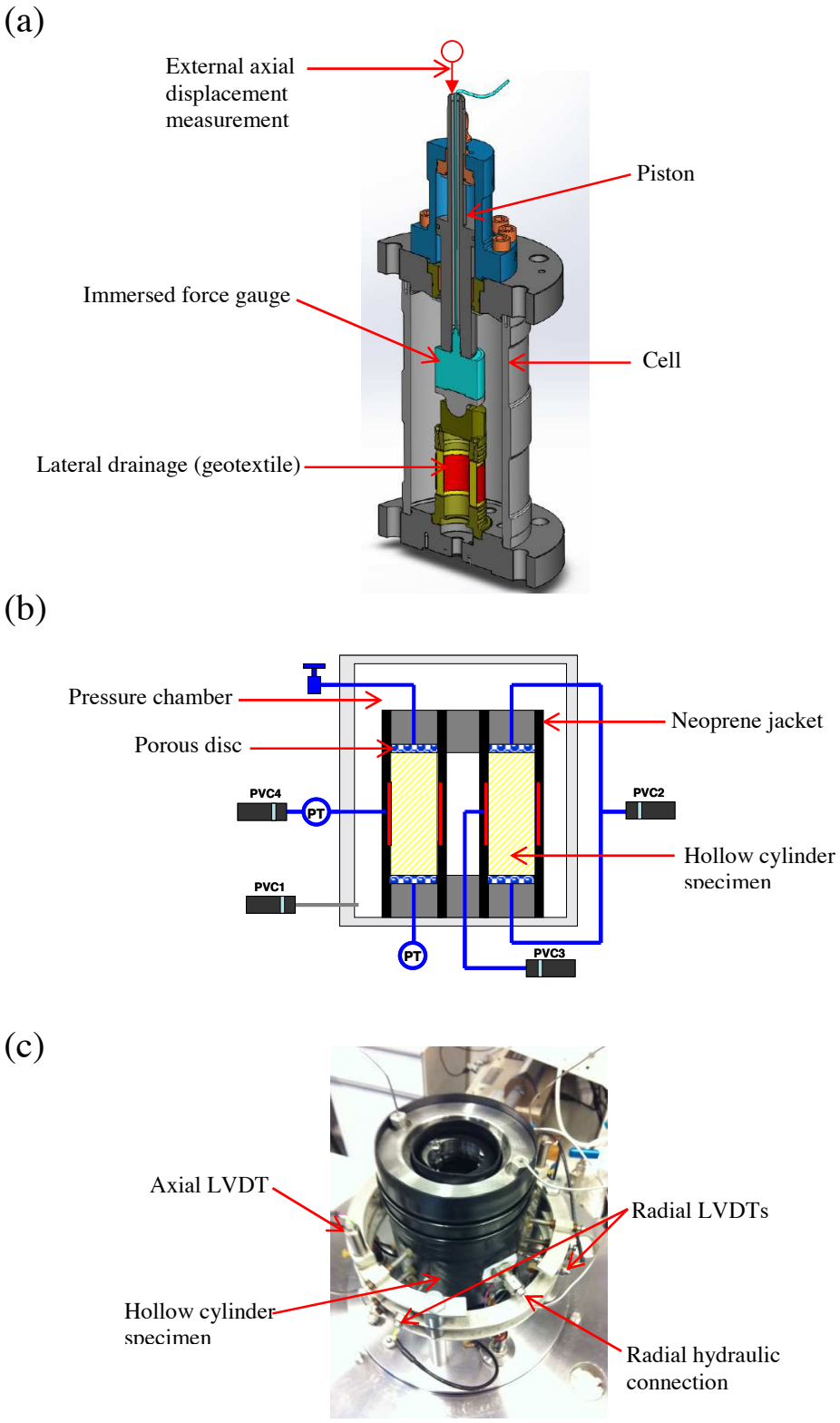

Fig. 2. (a): Hollow cylinder triaxial cell, (b): Scheme of the hydraulic connections, (c): Local strain measurement system.

Figure 3

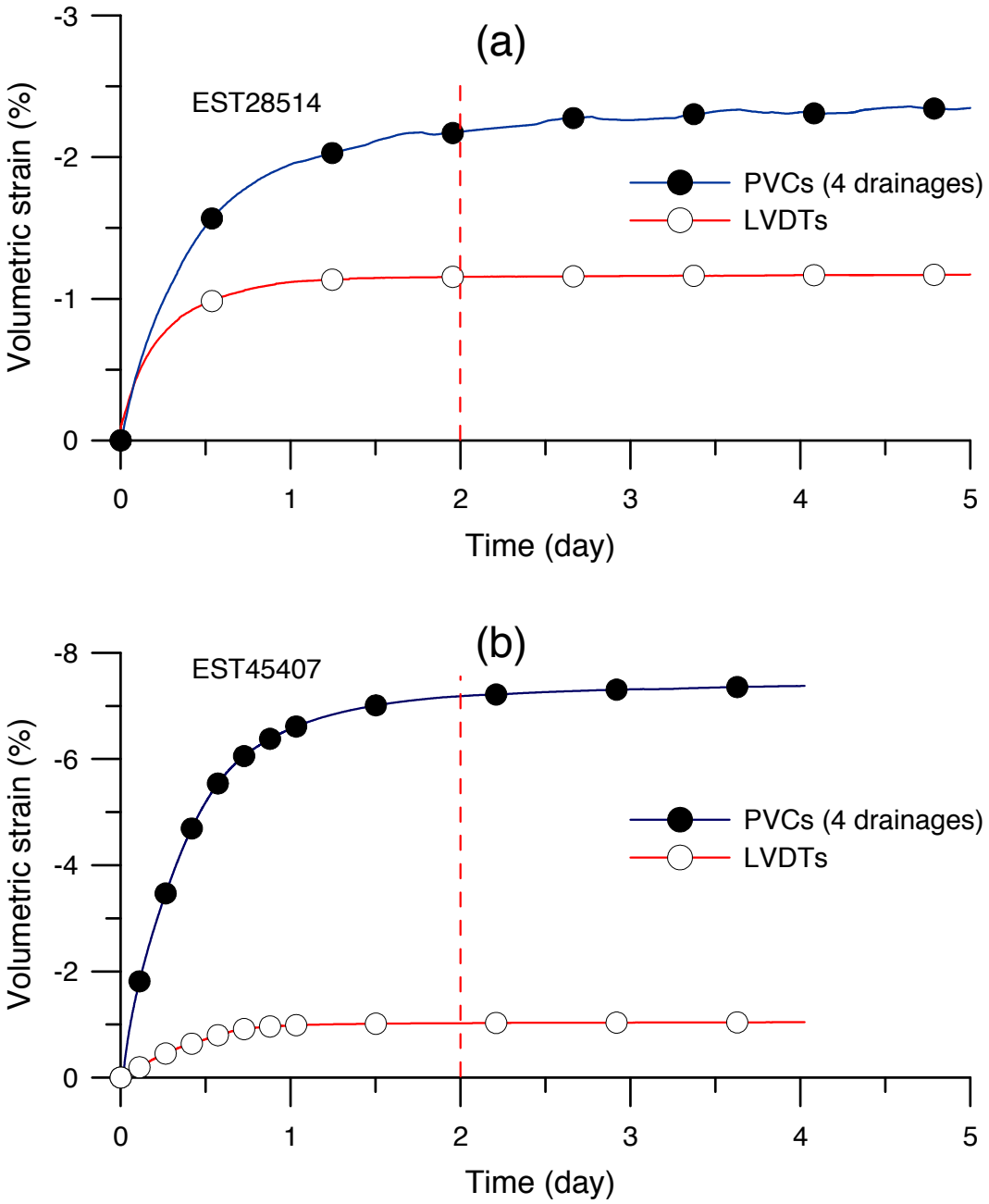

Fig. 3. Volume changes and water exchanges during resaturation phase; (a) test T3, (b) test T6.

Figure 4

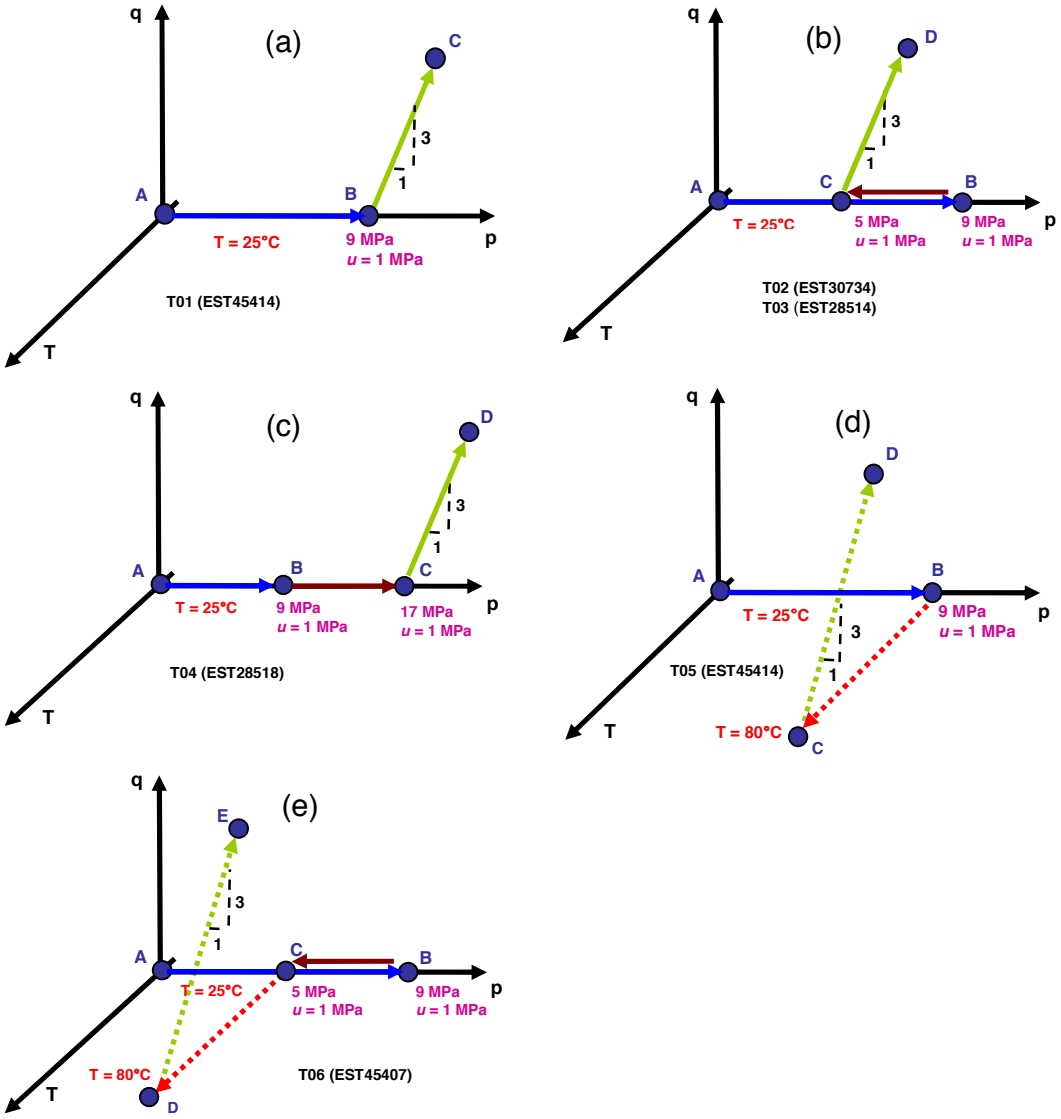

Fig. 4. Thermo-hydro-mechanical paths followed during the tests carried out.

Figure 5

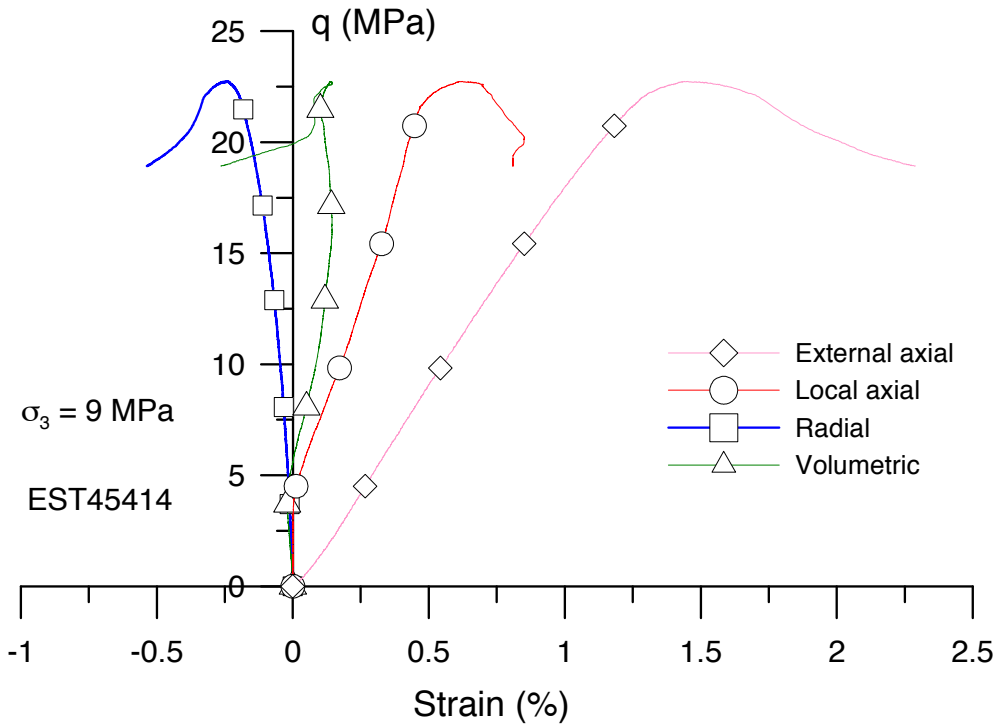

Fig. 5. Drained shear test under in-situ effective stresses at 25°C, test T1.

Figure 6

Fig. 6. COx claystone at the end of the test T1.

Figure 7

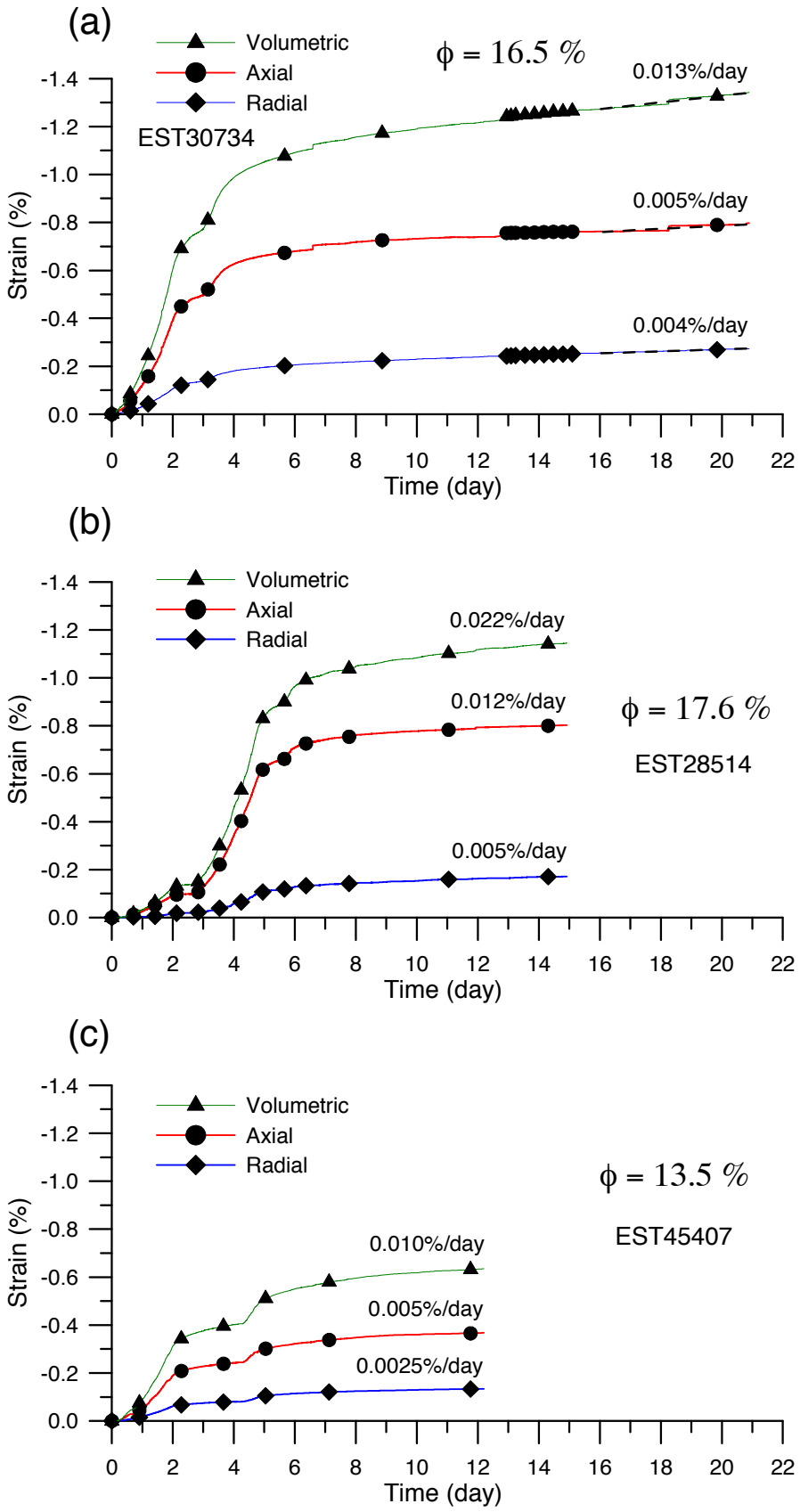

Fig. 7. Drained isotropic unloading phase, (a): T2, (b): T3, (c): T6.

Figure 8

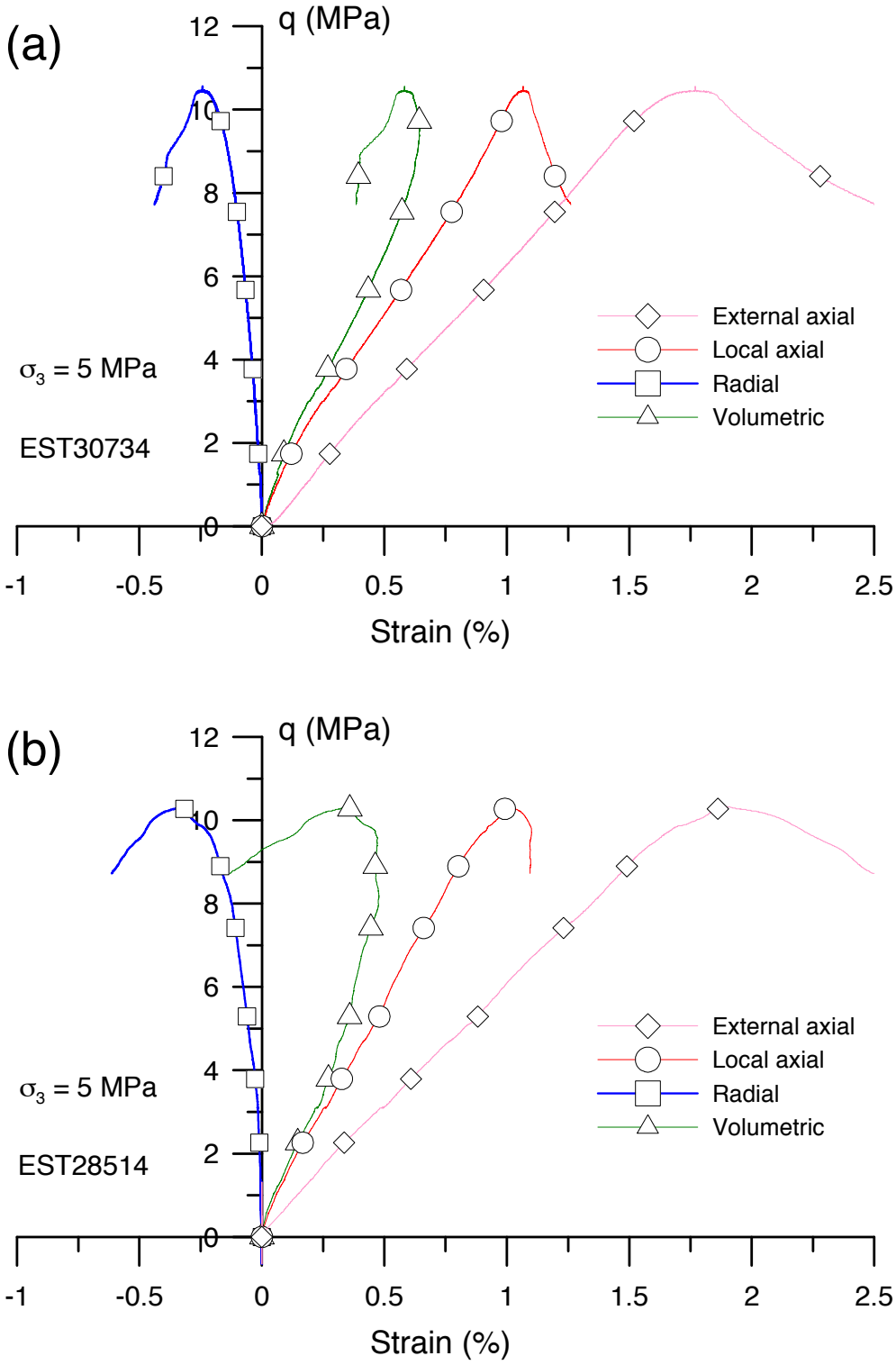

Fig. 8. Drained shear test under half in-situ effective stresses at 25°C, (a): test T2, (b): test T3.

Figure 9

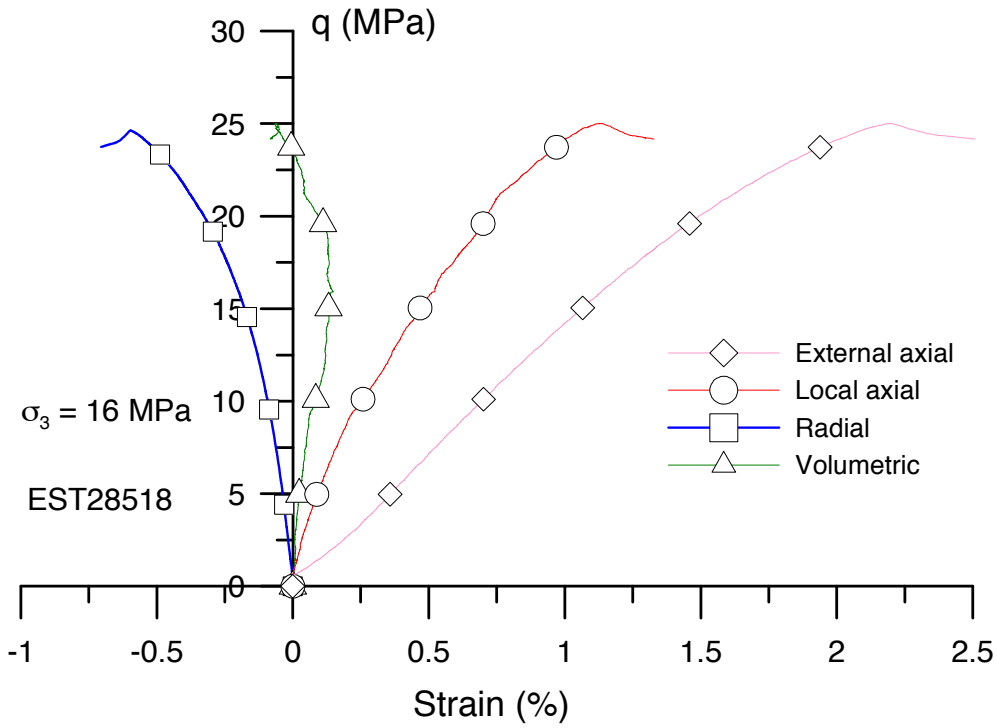

Fig. 9. Drained shear test under twice in-situ effective stresses at 25°C, test T4.

Figure 10

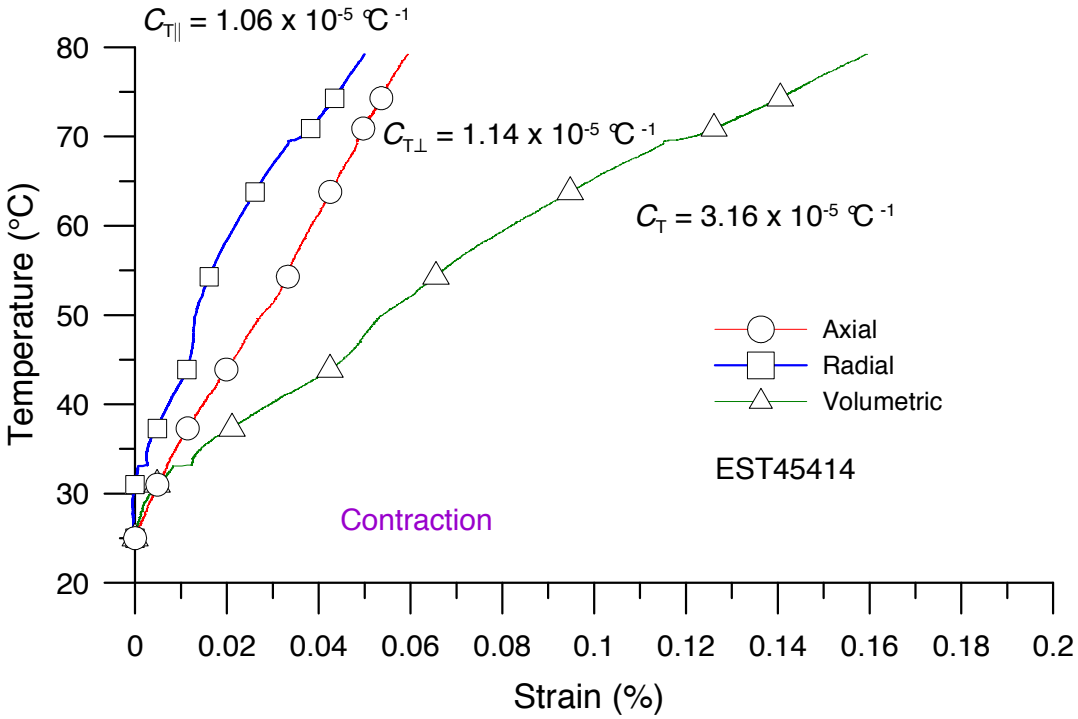

Fig. 10. Axial, radial and volumetric strains measured during a drained heating test (0.5°C/h) under in-situ effective stresses, test T5.

Figure 11

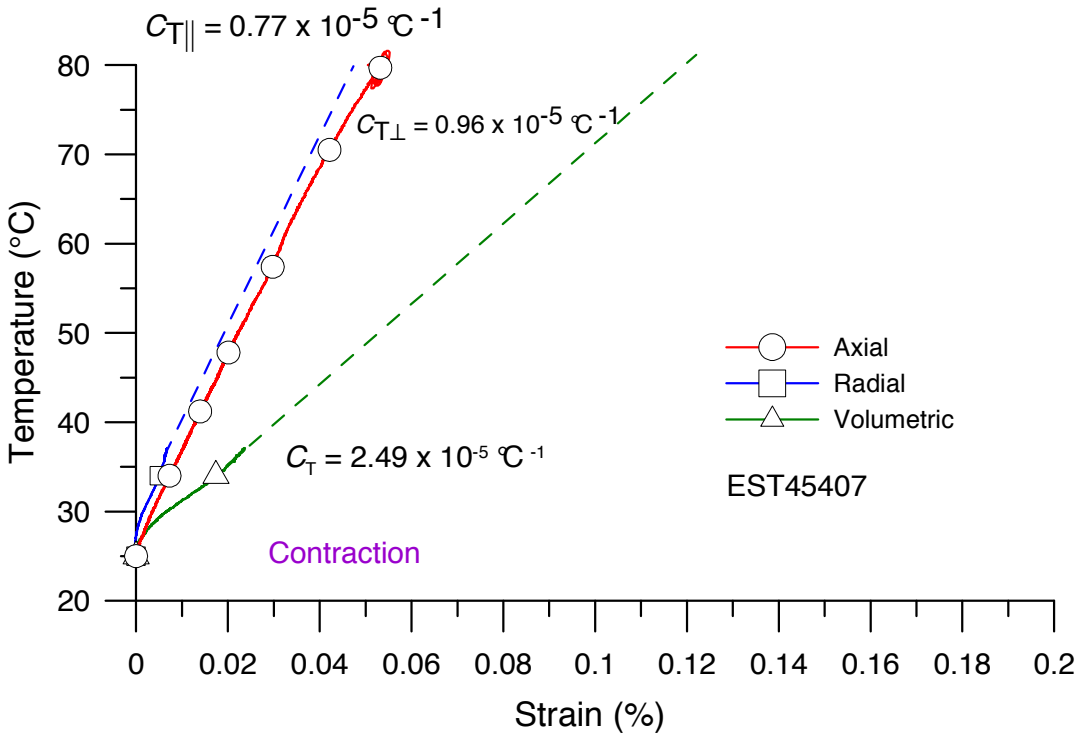

Fig. 11. Axial, radial and volumetric strains measured during a drained heating under half in-situ effective stresses, test T6.

Figure 12

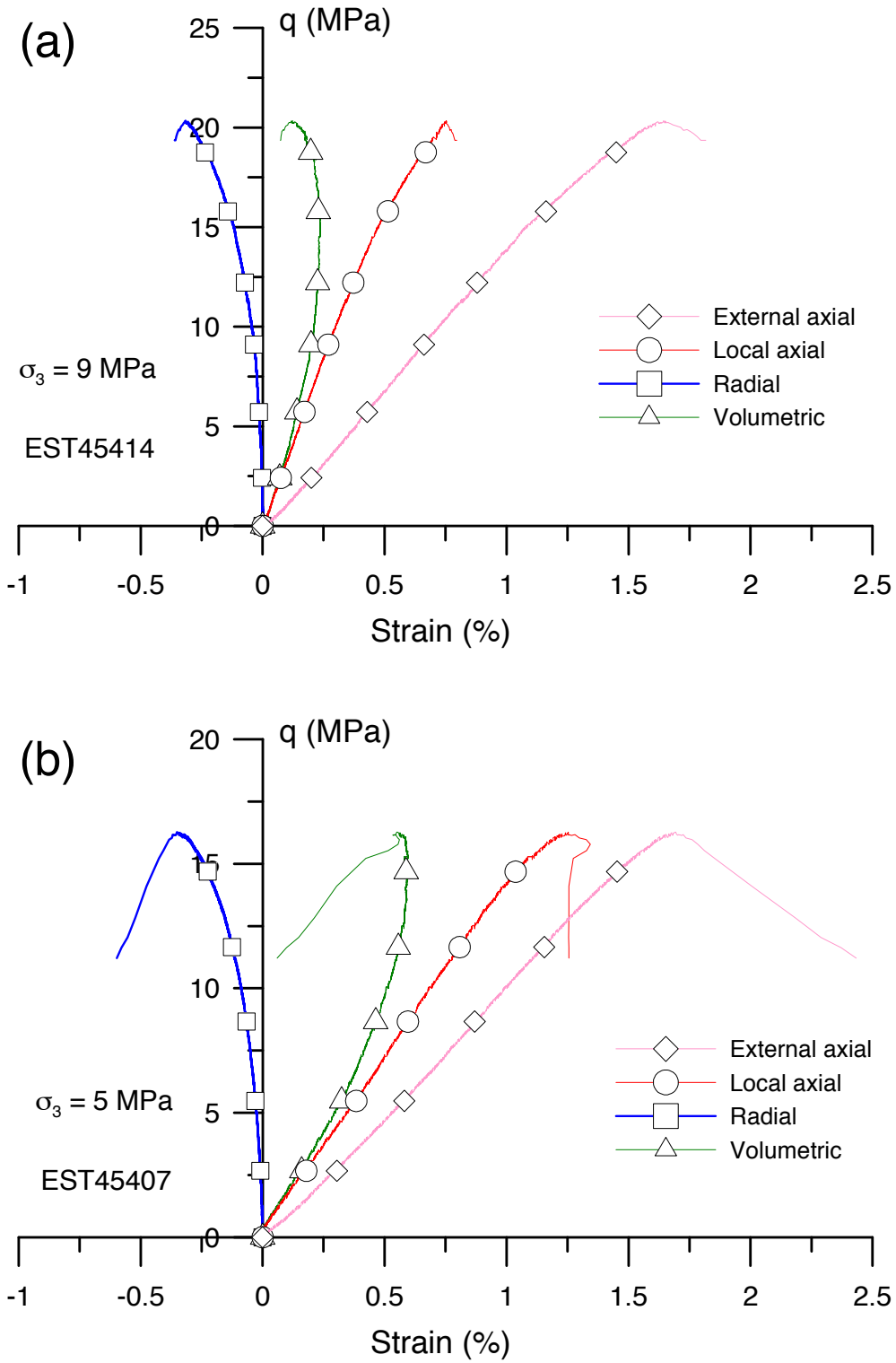

Fig. 12. Drained shear test at 80°C, (a): test T5, (b): test T6.

Figure 13

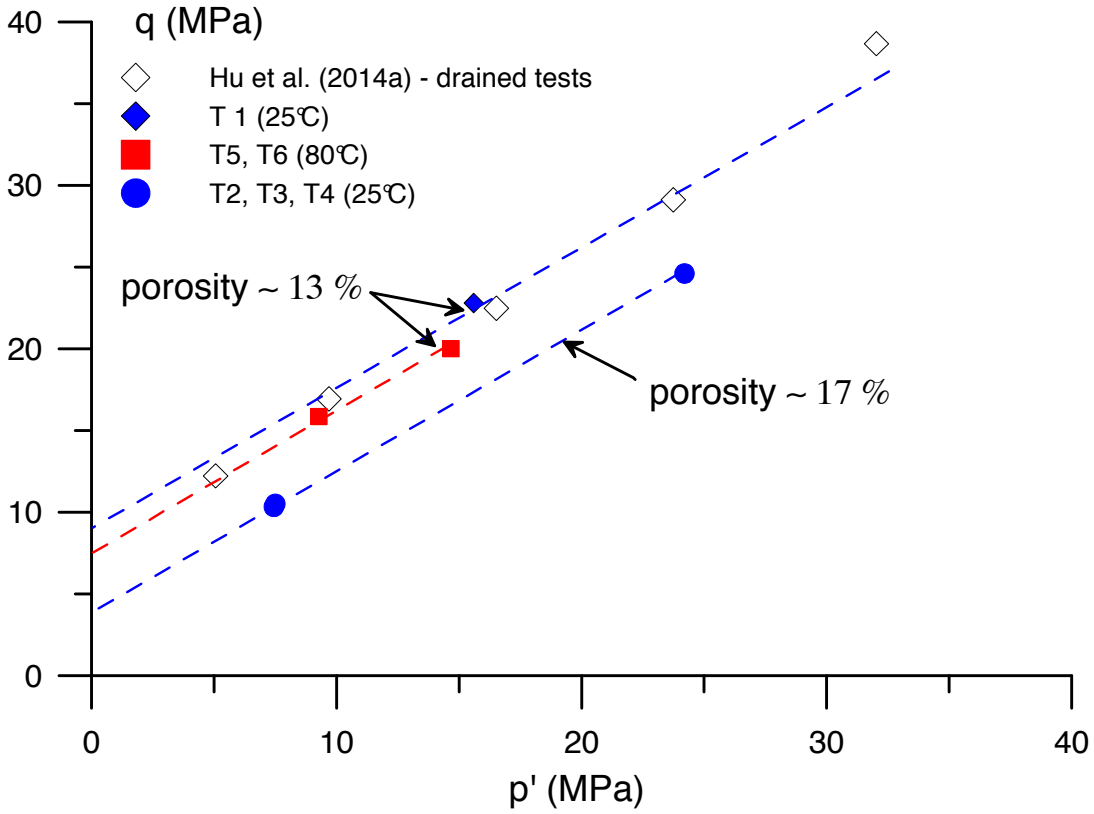

Fig. 13. Shear strength of all tests carried out in the plan q-p'.

Figure 14

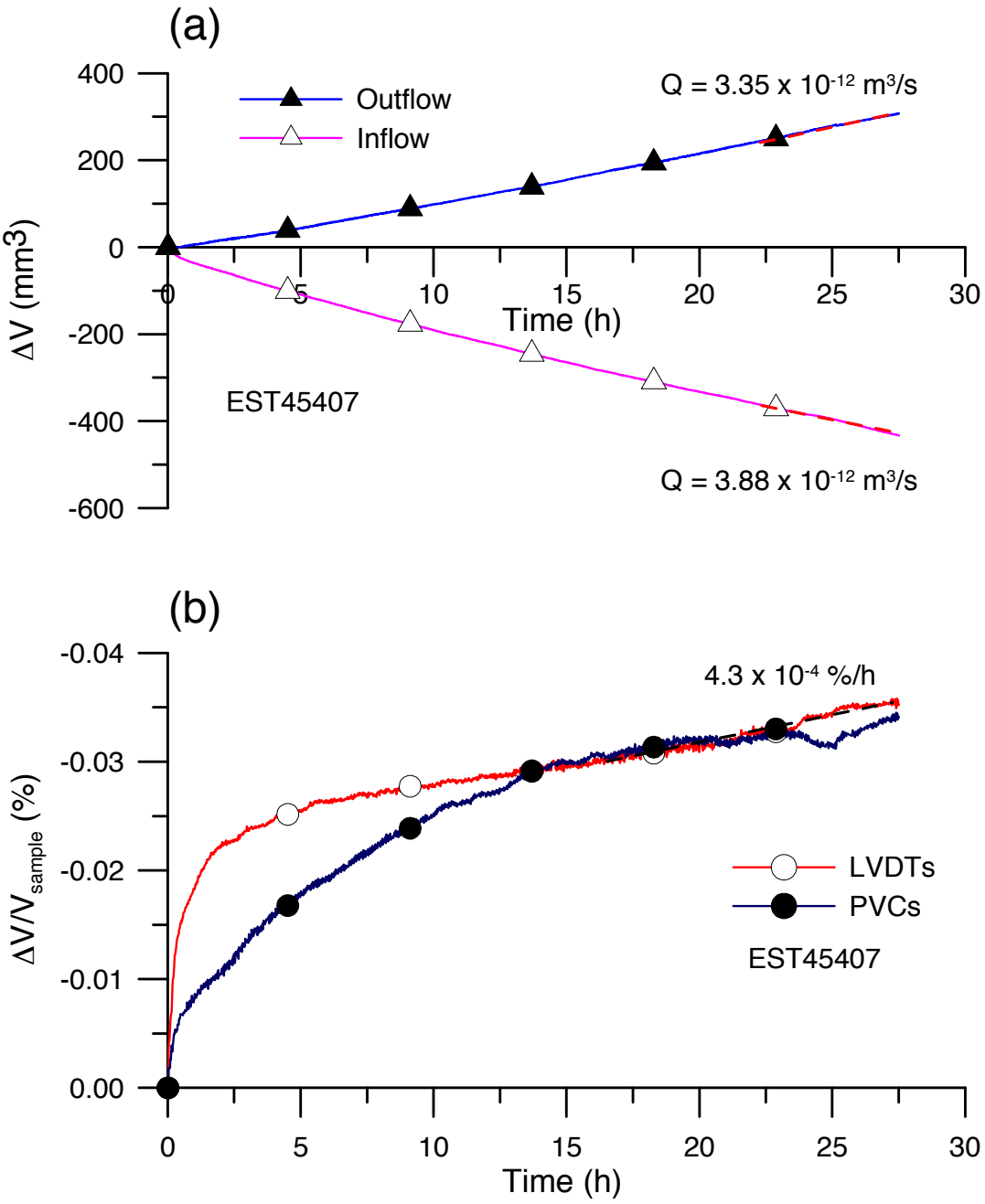

Fig. 14. Radial permeability test at point B, after resaturation T6, (a): inflow and outflow, (b): volume change.

Figure 15

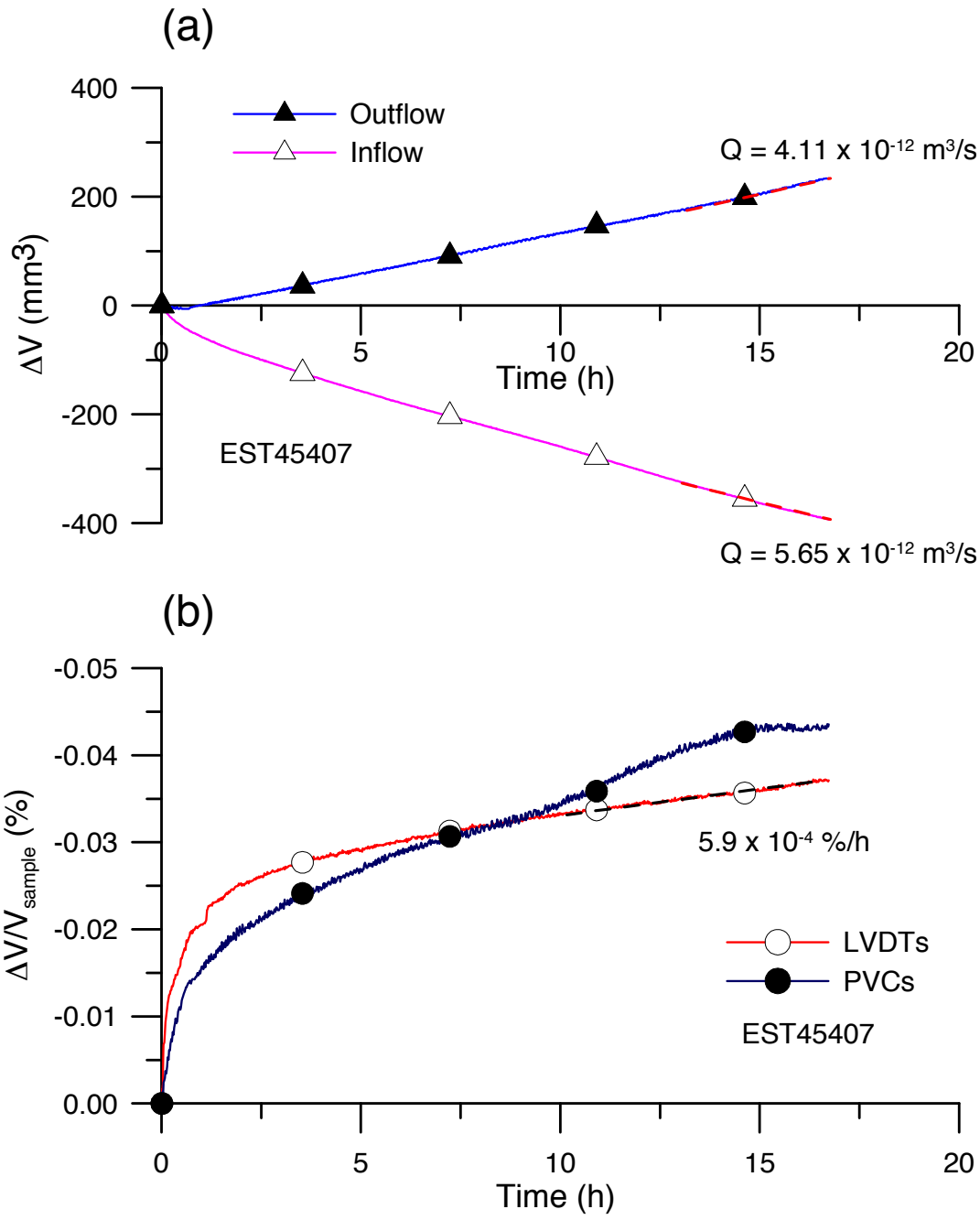

Fig. 15. Radial permeability test at point C, after swelling T6, (a): inflow and outflow, (b): volume change.

Figure 16

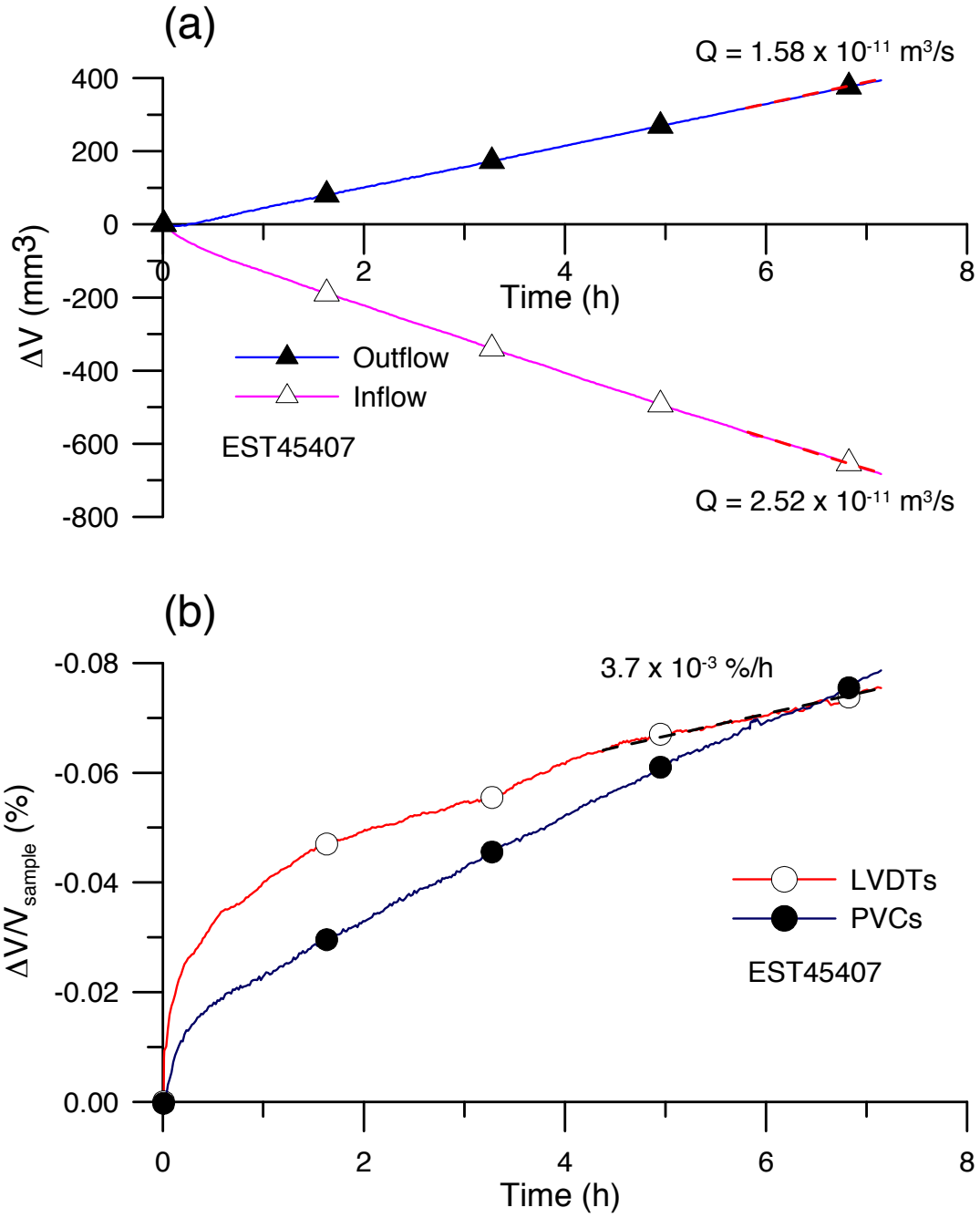

Fig. 16. Radial permeability test at point D, after heating T6, (a): inflow and outflow, (b): volume change.

Figure 17

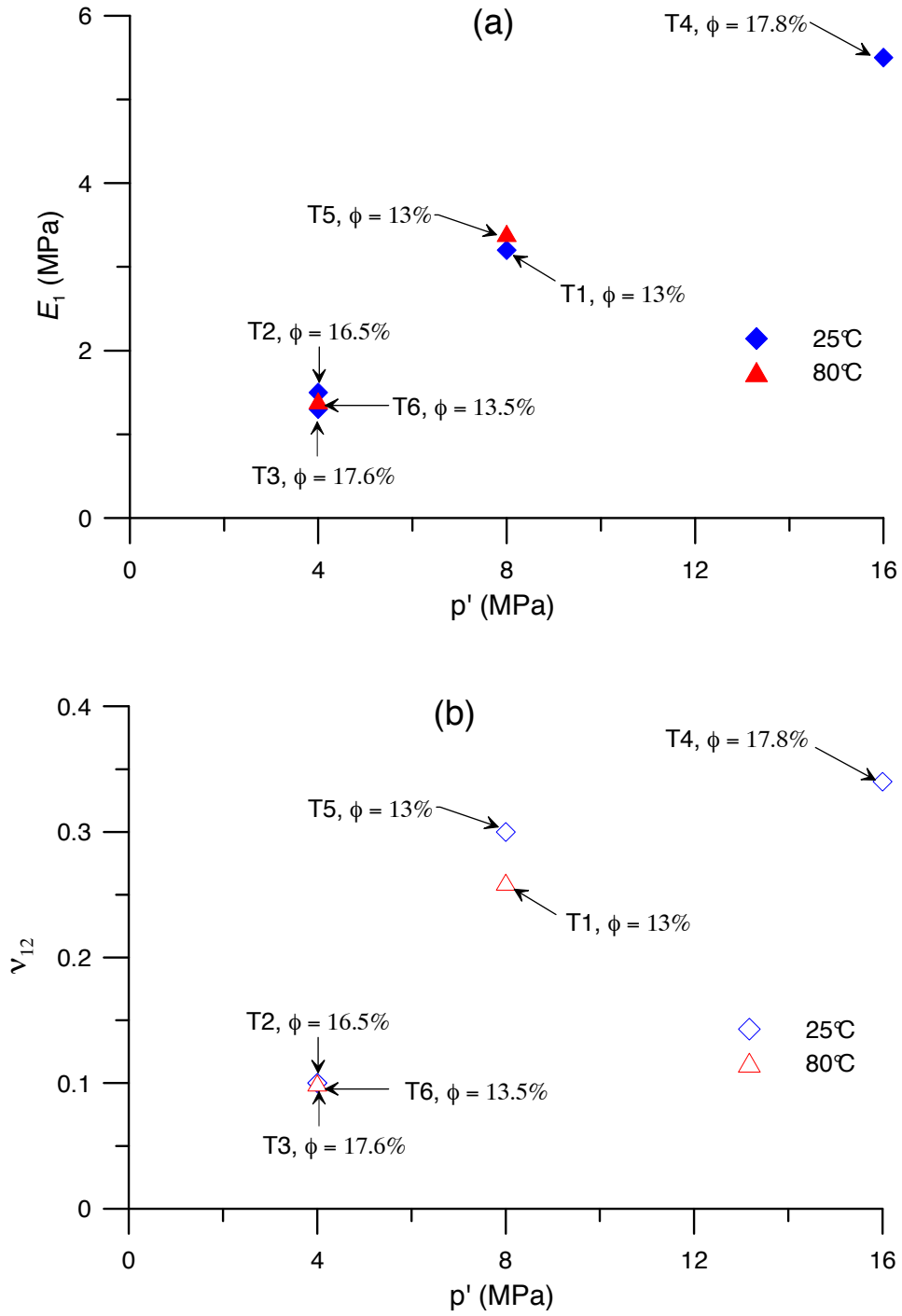

Fig. 17. Elastic parameters, (a): Young's modulus, (b): Poisson coefficient.